A Method of Moments Based Tool for the Analysis of Single Layer Loaded Microstrip Circuits and Antennas

by

Thomas N. Judge

76

A Thesis Presented to
the Faculty of Graduate Studies

University of Manitoba

In Partial Fulfillment of the Degree
Master of Science (EE)

September, 1995

National Library
of Canada

Acquisitions and
Bibliographic Services Branch

395 Wellington Street
Ottawa, Ontario
K1A 0N4

Bibliothèque nationale
du Canada

Direction des acquisitions et
des services bibliographiques

395, rue Wellington
Ottawa (Ontario)
K1A 0N4

Your file Votre référence

Our file Notre référence

ISBN 0-612-13229-3

Canada

Name _____

Dissertation Abstracts International is arranged by broad, general subject categories. Please select the one subject which most nearly describes the content of your dissertation. Enter the corresponding four-digit code in the spaces provided.

Electronics and Electrical Engineering
SUBJECT TERM

0544
SUBJECT CODE

U·M·I

Subject Categories

THE HUMANITIES AND SOCIAL SCIENCES

COMMUNICATIONS AND THE ARTS
Architecture 0729
Art History 0377
Cinema 0900
Dance 0378
Fine Arts 0357
Information Science 0723
Journalism 0391
Library Science 0399
Mass Communications 0708
Music 0413
Speech Communication 0459
Theater 0465

EDUCATION
General 0515
Administration 0514
Adult and Continuing 0516
Agricultural 0517
Art 0273
Bilingual and Multicultural 0282
Business 0688
Community College 0275
Curriculum and Instruction 0727
Early Childhood 0518
Elementary 0524
Finance 0277
Guidance and Counseling 0519
Health 0680
Higher 0745
History of 0520
Home Economics 0278
Industrial 0521
Language and Literature 0279
Mathematics 0280
Music 0522
Philosophy of 0998
Physical 0523
Psychology 0525
Reading 0535
Religious 0527
Sciences 0714
Secondary 0533
Social Sciences 0534
Sociology of 0340
Special 0529
Teacher Training 0530
Technology 0710
Tests and Measurements 0288
Vocational 0747

LANGUAGE, LITERATURE AND LINGUISTICS
Language
- General 0679
- Ancient 0289
- Linguistics 0290
- Modern 0291

Literature
- General 0401
- Classical 0294
- Comparative 0295
- Medieval 0297
- Modern 0298
- African 0316
- American 0591
- Asian 0305
- Canadian (English) 0352
- Canadian (French) 0355
- English 0593
- Germanic 0311
- Latin American 0312
- Middle Eastern 0315
- Romance 0313
- Slavic and East European 0314

PHILOSOPHY, RELIGION AND THEOLOGY
Philosophy 0422
Religion
- General 0318
- Biblical Studies 0321
- Clergy 0319
- History of 0320
- Philosophy of 0322

Theology 0469

SOCIAL SCIENCES
American Studies 0323
Anthropology
- Archaeology 0324
- Cultural 0326
- Physical 0327

Business Administration
- General 0310
- Accounting 0272
- Banking 0770
- Management 0454
- Marketing 0338

Canadian Studies 0385
Economics
- General 0501
- Agricultural 0503
- Commerce-Business 0505
- Finance 0508
- History 0509
- Labor 0510
- Theory 0511

Folklore 0358
Geography 0366
Gerontology 0351
History
- General 0578
- Ancient 0579
- Medieval 0581
- Modern 0582
- Black 0328
- African 0331
- Asia, Australia and Oceania 0332
- Canadian 0334
- European 0335
- Latin American 0336
- Middle Eastern 0333
- United States 0337

History of Science 0585
Law 0398
Political Science
- General 0615
- International Law and Relations 0616
- Public Administration 0617

Recreation 0814
Social Work 0452
Sociology
- General 0626
- Criminology and Penology ... 0627
- Demography 0938
- Ethnic and Racial Studies 0631
- Individual and Family Studies 0628
- Industrial and Labor Relations 0629
- Public and Social Welfare 0630
- Social Structure and Development 0700
- Theory and Methods 0344

Transportation 0709
Urban and Regional Planning 0999
Women's Studies 0453

THE SCIENCES AND ENGINEERING

BIOLOGICAL SCIENCES
Agriculture
- General 0473
- Agronomy 0285
- Animal Culture and Nutrition 0475
- Animal Pathology 0476
- Food Science and Technology 0359
- Forestry and Wildlife 0478
- Plant Culture 0479
- Plant Pathology 0480
- Plant Physiology 0817
- Range Management 0777
- Wood Technology 0746

Biology
- General 0306
- Anatomy 0287
- Biostatistics 0308
- Botany 0309
- Cell 0379
- Ecology 0329
- Entomology 0353
- Genetics 0369
- Limnology 0793
- Microbiology 0410
- Molecular 0307
- Neuroscience 0317
- Oceanography 0416
- Physiology 0433
- Radiation 0821
- Veterinary Science 0778
- Zoology 0472

Biophysics
- General 0786
- Medical 0760

EARTH SCIENCES
Biogeochemistry 0425
Geochemistry 0996
Geodesy 0370
Geology 0372
Geophysics 0373
Hydrology 0388
Mineralogy 0411
Paleobotany 0345
Paleoecology 0426
Paleontology 0418
Paleozoology 0985
Palynology 0427
Physical Geography 0368
Physical Oceanography 0415

HEALTH AND ENVIRONMENTAL SCIENCES
Environmental Sciences 0768
Health Sciences
- General 0566
- Audiology 0300
- Chemotherapy 0992
- Dentistry 0567
- Education 0350
- Hospital Management 0769
- Human Development 0758
- Immunology 0982
- Medicine and Surgery 0564
- Mental Health 0347
- Nursing 0569
- Nutrition 0570
- Obstetrics and Gynecology .. 0380
- Occupational Health and Therapy 0354
- Ophthalmology 0381
- Pathology 0571
- Pharmacology 0419
- Pharmacy 0572
- Physical Therapy 0382
- Public Health 0573
- Radiology 0574
- Recreation 0575
- Speech Pathology 0460
- Toxicology 0383

Home Economics 0386

PHYSICAL SCIENCES
Pure Sciences
Chemistry
- General 0485
- Agricultural 0749
- Analytical 0486
- Biochemistry 0487
- Inorganic 0488
- Nuclear 0738
- Organic 0490
- Pharmaceutical 0491
- Physical 0494
- Polymer 0495
- Radiation 0754

Mathematics 0405
Physics
- General 0605
- Acoustics 0986
- Astronomy and Astrophysics 0606
- Atmospheric Science 0608
- Atomic 0748
- Electronics and Electricity 0607
- Elementary Particles and High Energy 0798
- Fluid and Plasma 0759
- Molecular 0609
- Nuclear 0610
- Optics 0752
- Radiation 0756
- Solid State 0611

Statistics 0463

Applied Sciences
Applied Mechanics 0346
Computer Science 0984
Engineering
- General 0537
- Aerospace 0538
- Agricultural 0539
- Automotive 0540
- Biomedical 0541
- Chemical 0542
- Civil 0543
- Electronics and Electrical 0544
- Heat and Thermodynamics ... 0348
- Hydraulic 0545
- Industrial 0546
- Marine 0547
- Materials Science 0794
- Mechanical 0548
- Metallurgy 0743
- Mining 0551
- Nuclear 0552
- Packaging 0549
- Petroleum 0765
- Sanitary and Municipal 0554
- System Science 0790

Geotechnology 0428
Operations Research 0796
Plastics Technology 0795
Textile Technology 0994

PSYCHOLOGY
General 0621
Behavioral 0384
Clinical 0622
Developmental 0620
Experimental 0623
Industrial 0624
Personality 0625
Physiological 0989
Psychobiology 0349
Psychometrics 0632
Social 0451

A METHOD OF MOMENTS BASED TOOL FOR THE ANALYSIS OF SINGLE LAYER LOADED MICROSTRIP CIRCUITS AND ANTENNAS

BY

THOMAS N. JUDGE

A Thesis submitted to the Faculty of Graduate Studies of the University of Manitoba in partial fulfillment of the requirements of the degree of

MASTER OF SCIENCE

I hereby declare that I am the sole author of this thesis.

I Authorize the University of Manitoba to lend this thesis to other institutions or individuals for the purpose of scholarly research.

I further authorize the University to reproduce this thesis by photocopying or other means, in total or in part, at the request of other institutions or individuals for the purpose of scholarly research.

Abstract

The Method of Moments is used for the development of a tool for analysing the input impedance characteristics and radiation patterns of an arbitrarily shaped microstrip structure. Input reflection coefficients are obtained for line fed structures as well as input impedances for those fed by coaxial cable. A simple method for characterizing loads between structures and loads from the structure to the ground plane is given as well as a simple model for characterizing an active device between structures. Numerical results are compared to solutions obtained using analytic methods as well as results measured by other researchers. A consistent accuracy of less than 5% is obtained for regular geometries and methods for improving the result for irregular structures are outlined.

Acknowledgements

I would like to express my gratitude to Dr. A. Sebak for his suggestion of this project, for his many invaluable suggestions through out the course of my study, and for his patience.

Financial support received through Dr G. Bridges and Micronet, and Dr. L. Shafai are also gratefully acknowledged

I would also like to thank several of my colleagues, especially Mr. Ming Zhang for consultation on various mathematical matters and Mr. Cameron W. Mayor for helping to provide a pleasant working atmosphere, as well as others too many to name who contributed so much.

Finally, I would like to express my sincere gratitude and love to my parents for instilling in me the work ethic and teaching me the patience required for the completion of such a project and especially to my wife Bonnie for always being there and for understanding when I was not.

Table of Contents

Table of Figures

Figure **Page**

List of Principal Symbols

Symbol	Meaning
c	speed of light in free space
ε_0	permittivity of free space
μ_0	permeability of free space
ε_r	relative permittivity of a material (dielectric)
σ	conductivity of a material
f	frequency of excitation
λ_0	free space wavelength = c/f
λ_d	dielectric wavelength = $c/\left(f\sqrt{\varepsilon_r}\right)$
ω	angular frequency = $2\pi f$
$\grave{\mathbf{E}}$	electric field vector
$\grave{\mathbf{E}}^s$	scattered electric field
$\grave{\mathbf{E}}^i$	impressed electric field
$\grave{\mathbf{J}}_s$	surface current density
ρ_s	surface charge density
Z_s	surface impedance of a conductor
Z_L	load impedance
$Z_{11}, Z_{21}, Z_{12}, Z_{22}$	components of an active device Z-matrix
$\grave{\mathbf{H}}$	magnetic field intensity vector

$\vec{\mathbf{A}}$	magnetic vector potential
V	scalar electric potential
G_V	Green's function for the electric scalar potential
$\overrightarrow{\overrightarrow{\mathbf{G}}}_A$	dyadic Green's function for the magnetic vector potential
k	wave number = $2\pi/\lambda$
$J_0(x)$	Bessel function of order 0 of x
$J_1(x)$	Bessel function of order 1 of x
h	height of the dielectric substrate
(x_s, y_s, z_s)	x, y, z cartesian coordinates of source point
(x_o, y_o, z_o)	x, y, z cartesian coordinates of observation point
$\tan\delta$	loss tangent of the dielectric material
$\delta(x)$	Dirac delta function
$\Delta x, \Delta y, \Delta z$	the x, y and z dimensions of a charge cell
N_x, N_y, N_z	number of current cells on a surface conductor in the x, y and z directions
$\vec{r}$	vector joining the origin to an observation point
$\vec{r}'$	vector joining the origin to a source point
T_x, T_y, T_z	triangular rooftop basis functions in the x, y, and z directions
Π	pulse basis function
β	the propagation constant on a microstrip line
SWR	the standing wave ratio on the microstrip line
Γ_{in}	the input reflection coefficient of a microstrip circuit
$\phi(\Gamma_{in})$	phase of the input reflection coefficient
$[Z]$	the impedance matrix of the system

$[V]$	the excitation vector of the system consisting of the line integrals of the impressed electric field
$[I]$	the solution vector of the system consisting of the coefficients of the current basis functions
Z_{in}	the input impedance of the microstrip circuit or antenna

1 Introduction

1.1 Background and Motivation

The introduction of microwave integrated circuit (MIC) technology in the early 1950's has drastically changed the face of microwave engineering. With this technology, transmission elements and discrete components are mounted together as with the more common digital printed circuit board technology. By contrast, using the more traditional microwave technologies, circuits are formed by connecting discrete components through coaxial cables or waveguides. An obvious advantage is gained by having all components of a circuit mounted in one package as opposed to having them distributed between large transmission line sections [1].

There are, in MIC technology, several possibilities for the configuration of the transmission line elements [2]. Among the common configurations are stripline, where a central conductor is sandwiched between two ground plane backed dielectric substrates, as seen in figure 1.1.1A, coplanar waveguide, where the ground planes are placed adjacent to the centre conductor on the dielectric, as seen in figure 1.1.1B, and slotline, where the signal is transmitted in the slot between two conductors on a dielectric, as shown in figure 1.1.1C. By far the most widely used format, however, is the microstrip transmission line, as shown in figure 1.1.2. The microstrip format consists of a conductor mounted on a dielectric substrate backed by a ground plane. Benefits of this format over the others include its simplicity of fabrication and the access allowed to the surface conductor for

placing and adjusting discrete components. One of the main drawbacks of microstrip however, is unwanted radiation and coupling to other elements on the same substrate. It has become very important to designers of MIC devices to find the minimum distance required between transmission elements that will result in an acceptable level of signal corruption due to the coupling of the lines (also known as cross-talk).

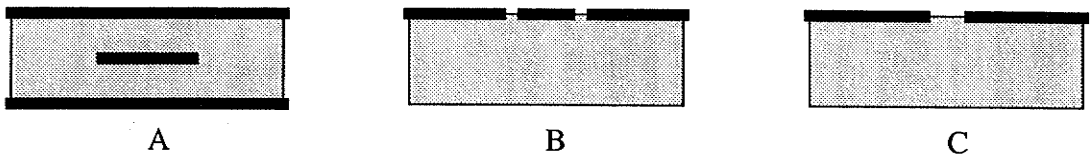

Fig. 1.1.1 Stripline (A), Coplanar Waveguide (B) and Slotline (C) Transmission Lines

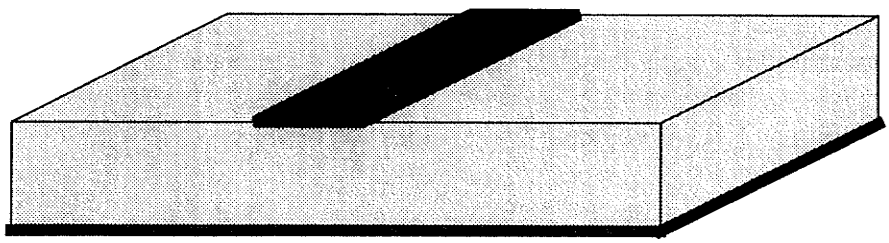

Fig. 1.1.2 Microstrip Transmission Line Format

Also in the early 1950's, a conductor supported by a ground plane backed dielectric substrate was first proposed as a radiating element [3]. The radiator is referred to as a microstrip antenna due to its similarity to microstrip transmission lines. Since this time, literally countless investigations have been carried out on variations of this main theme, as enumerated by Lo et al.[4]. These variations include both resonant type antennas, such as the rectangular patch [5], the circular disc [6] and microstrip dipoles [7], and travelling wave type antennas [8]. Microstrip antennas, however, suffer from a number of deficiencies which make them unattractive for some applications. One problem incurred in using microstrip patch antennas is the inherently low bandwidth. Experiments into resolving this problem have included reactive loading of the patch antenna [9], [10] or placing parasitic elements near to it [11], [12] to increase the impedance bandwidth. Perturbations of the basic geometry may also be used to increase the bandwidth or to enable diversity in the polarization. Linear and planar arrays of microstrip patch elements are often used to increase the radiated power and achieve a more directed beam [13]. Recently, MIC technology has been combined with microstrip antennas to form active antennas and active arrays which may also solve some of these problems [14], [15].

The vast majority of the aforementioned antenna designs have been developed by researchers who have used their own intuitive knowledge and some empirical data to conceptualize their designs and then physically build and test them. Perfecting the design in this manner is generally a very time consuming and costly procedure. For this reason, the ability to perform accurate numerical analyses on microstrip structures, in general, has gained a great deal of interest by antenna and circuit designers alike. To provide a tool that

will be useful and relevant to both circuit and antenna designs which are currently being investigated, the method of analysis requires generality, accuracy at higher frequencies, and the ability to derive multiple characteristics from the results.

Several analysis techniques are currently in use for these types of problems. A good enumeration of these is given by Itoh [16]. Many methods such as cavity models, mode matching method and the multiport network model (or planar circuit method) rely on standard geometries, the effort to include the kind of generality desired here is not trivial. Others model the relationships between current and voltage on these structures such as the transmission line matrix method [17]. Using such a model, coupling and fringing effects may be ignored or at least difficult to model. Still others, such as the microwave circuit simulators TOUCHSTONE and Puff rely on static approximations which may not be valid at the frequencies which today's curcuits and antennas operate. Often, a full wave analysis is required which approximates the actual fields and takes into account high frequency and coupling effects. To this end, the Method of Moments [18] has been used in many electromagnetic scattering and radiation problems. Here, the requirement is for a formulation that is specific to the microstrip problem but general enough to handle arbitrary geometries operating under arbitrary feeding and loading conditions.

1.2 Objectives

This work was initiated in order to provide a tool for the analysis of single layer microstrip circuits and antennas loaded with passive or active components. The main objective in designing the tool is to enable analysis on as general a design as possible, combining arbitrary geometries with arbitrary loading and active element integration as represented by the active array in figure 1.2.1. In order to provide information that will be relevant to designers, the input impedance, far-field radiation patterns and current distributions are all sought. A secondary objective of the project is to provide a starting point for the continuing design of tools to analyse more complex, for example multiple layered, structures. A final consideration in the design of such a tool is to ensure that it is easy to use and that the time and computer memory required for the analysis of a realistic design is not prohibitive to the use of the tool.

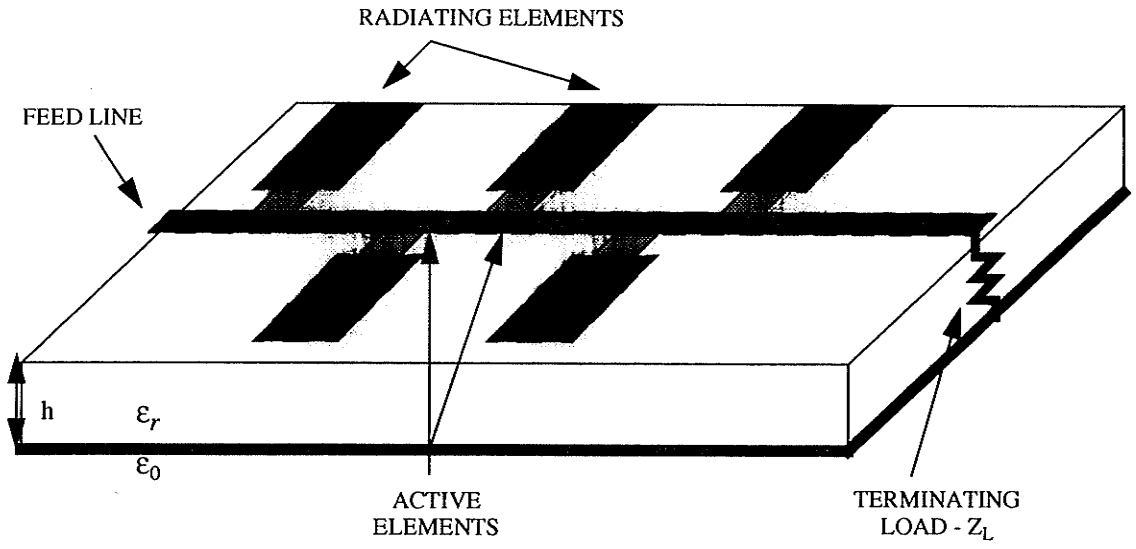

Fig. 1.2.1 A Planar Array Incorporating Active Elements and a Terminating Load

This document is presented in six sections. Following this section, the formulation of the problem and the Green's Functions, which are the kernel of the integral equations solved by the Method of Moments, are described. In the third section the application of the Method of Moments as it applies to this problem is discussed. The method of calculating the far field radiation patterns using asymptotic expressions for the Green's functions are also included in this third section. Special considerations are then given for dealing with different types of excitation, placing passive loads on the structures and integrating the microstrip structures with active devices. The fifth section presents some numerical results and compares them with analytic approximations and previously published data. Finally, the validity of the results are discussed along with other considerations including computer efficiency. This final section also includes a discussion of further study that may be appended to the current work

1.3 Comments and Assumptions

In this study of single layer microstrip structures, the ideal of generality is sought throughout. Some assumptions, however, must be made in order to facilitate the formulation and subsequent numerical approximation of the solution. These include:

- ground plane and substrate are approximated to extend infinitely
- the substrate itself is assumed to be linear, isotropic and homogeneous but, in general, lossy
- the ground plane is assumed to be a perfect conductor
- surface conductors are assumed to be infinitely thin

Finally, the solution is performed in the frequency domain and therefore the a time variation of $e^{j\omega t}$ is assumed and suppressed throughout the formulation and solution.

2 The Mixed Potential Integral Equation

2.1 Integral Equation Formulation

The boundary condition for the total electric field with respect to the arbitrarily shaped conducting parts of the structure is given in equation 2.1.1 below [19]. When the conductors are perfect, the total electric field tangent to the conductor surface is zero. Here, the right hand side of the equation reflects the ohmic loss that occurs when then conductors are not perfectly conducting.

$$\hat{n} \times \left(\vec{\mathbf{E}}^{s}(\vec{r}) + \vec{\mathbf{E}}^{i}(\vec{r}) \right) = \hat{n} \times Z_s \vec{\mathbf{J}}_s(\vec{r}) \tag{2.1.1}$$

In this expression, $\vec{\mathbf{E}}^{s}$ and $\vec{\mathbf{E}}^{i}$ are the scattered and impressed electric field vectors respectively, Z_s is the surface impedance of the conductor, taken to be the classic surface impedance of the conductor $(1+j)\sqrt{\frac{\mu_0 f}{\pi\sigma}}$ and $\vec{\mathbf{J}}_s$ is the current density on the conductor.

The scattered electric field can be expressed using a scalar electric potential, *V*, and a magnetic vector potential, $\vec{\mathbf{A}}$ [20]. In order for a vector to be defined, however, both the curl and divergence must be defined. Hence, we define $\vec{\mathbf{A}}$, by relating the curl to the magnetic field intensity, $\vec{\mathbf{H}}$:

$$\vec{\mathbf{H}} = \nabla \times \vec{\mathbf{A}} \tag{2.1.2}$$

and the divergence to the scalar electric potential, *V:*

$$\nabla \cdot \vec{\mathbf{A}} = -j\omega\varepsilon V \tag{2.1.3}$$

The latter of which is known as the Lorentz Gauge [21].

It then follows from Maxwell's Equations that

$$\vec{\mathbf{E}}^{s}(\vec{r}) = -j\omega\vec{\mathbf{A}}(\vec{r}) - \nabla V(\vec{r}) \tag{2.1.4}$$

By replacing the scattered field by its scalar and vector potential representation (2.1.4) in the equation expressing the boundary condition (2.1.1)

$$\hat{n} \times \vec{\mathbf{E}}^{i}(\vec{r}) = j\omega(\hat{n} \times \vec{\mathbf{A}}(\vec{r})) + \nabla V(\vec{r}) + Z_s(\hat{n} \times \vec{\mathbf{J}}_s(\vec{r})) \tag{2.1.5}$$

The potentials can be further expressed as superposition integrals of the surface currents and charges with the Green's functions, which are responses to elemental sources.

$$\vec{\mathbf{A}}(r) = \iint_S \left[\overline{\overline{\mathbf{G}}}_A(\vec{r}|\vec{r}')\right] \cdot \vec{\mathbf{J}}_s(\vec{r}')\, dS' \tag{2.1.6}$$

$$V(r) = \iint_S G_V(\vec{r}|\vec{r}')\, \rho_s(\vec{r}')\, dS' \tag{2.1.7}$$

The Green's functions ($\left[\overline{\overline{\mathbf{G}}}_A(\vec{r}|\vec{r}')\right]$ and $G_V(\vec{r}|\vec{r}')$) represent the vector and potentials due to an infinitesimal current element and point charge respectively. These are discussed in the next section, along with the techniques used to calculate them. By inserting the superposition integrals (2.1.6) and (2.1.7) into the altered version of the boundary

condition equation (2.1.5) the following expression is obtained.

$$\vec{\mathbf{E}}^{i}(\vec{r}) = j\omega\iint_{S}\overline{\overline{\mathbf{G}}}_{A}(\vec{r}|\vec{r}')\cdot\vec{\mathbf{J}}_{s}(\vec{r}')\,dS' + \nabla\iint_{S}G_{V}(\vec{r}|\vec{r}')\,\rho_{s}(\vec{r}')\,dS' + Z_{s}\vec{\mathbf{J}}_{s}(\vec{r}) \qquad (2.1.8)$$

This equation is referred to as the Mixed Potential Integral Equation (MPIE) and, as will be seen in a future chapter, it is to this that the Method of Moments is applied

2.2 Green's Functions for Layered Media

In solving the fields in layered media, two approaches may be taken. The first uses the well known free space Green's functions, which is expressed in spherical coordinates by

$$G(\vec{r}|\vec{r}') = \frac{e^{-jk(|r-\vec{r}'|)}}{4\pi|\vec{r}-\vec{r}'|}. \qquad (2.2.1)$$

Using this method fictive electric and magnetic currents are used to describe the surface and volume effects which occur in the system. These fictive sources, however, are extra unknowns in the numerical solution and must be solved for [22]. The second, and more preferable approach, is to use Green's functions specially formulated for the particular combination of media present and therefore eliminate the requirement of fictive sources. These specialized Green's functions were first introduced by Sommerfeld [23], to describe radio waves propagating over lossy ground. Surface waves and dielectric losses are then accounted for in the Green's functions and only the currents and charges existing on the conductors are to be solved for using numerical methods.

The vector potential in inhomogeneous media may not necessary be parallel to the current that produces it [24]. In this case, it is convenient to express the Green's function as a *dyadic* as shown below.

$$d\vec{\mathbf{A}}(\vec{r}) = \vec{\vec{\mathbf{G}}}_A(\vec{r}|\vec{r}') \cdot \vec{\mathbf{J}}_s(\vec{r}')\, dr' \tag{2.2.2}$$

This is expressed in matrix form as

$$\begin{bmatrix} dA_x \\ dA_y \\ dA_z \end{bmatrix} = \begin{bmatrix} G_A^{xx} & G_A^{xy} & G_A^{xz} \\ G_A^{yx} & G_A^{yy} & G_A^{yz} \\ G_A^{zx} & G_A^{zy} & G_A^{zz} \end{bmatrix} \cdot \begin{bmatrix} J_{sx} dr' \\ J_{sy} dr' \\ J_{sz} dr' \end{bmatrix} \tag{2.2.3}$$

For a homogeneous medium, the vector potential and currents are same-directed, thus the dyadic Green's function maintains this form except that $G_A^{st} = G$ when $s=t$, with G the Green's function for the homogeneous medium, and $G_A^{st} = 0$ when $s \neq t$. In a layered medium, as is studied here, it has been shown that the vector potential produced by a current on the interface of the layered media can be described by two orthogonal vectors and that the vector potential produced by a current perpendicular to the interface requires only one component vector which is parallel to the current [24].

The Green's functions for both the scalar and vector potentials are derived by solving the homogeneous Helmholtz equations subject to the boundary conditions relevant to the geometry.

$$\left(\nabla^2 + k^2\right)\vec{\mathbf{A}} = 0 \tag{2.2.4}$$

$$\left(\nabla^2 + k^2\right)V = 0 \tag{2.2.5}$$

As the geometry under consideration is homogeneous in the transverse (x & y) directions and inhomogeneous in the vertical (z) direction these equations are solved in cylindrical coordinates. The solution involves the consideration of two cases. The first is to find the Green's functions in the transverse directions. A horizontal electric dipole (HED) is considered. The HED has current, I, and infinitesimal length dl and exists on the interface of the dielectric substrate and the air. The second case considered is that of a vertical electric dipole (VED) that has the same properties as the HED but is oriented perpendicular to the interface and is embedded in the dielectric substrate. The solution of the Green's function invokes a transformation to the spectral domain followed by a separation of variables solution of the differential (Helmholtz) equation, and then an inverse transformation back to the space domain. Analytical solutions have been solved for both cases of the current and the for the charges on the interface and embedded in the substrate by several authors [24], [25] and will not be repeated here. Instead, they are manipulated from these sources into a form that is convenient for calculation using the numerical method described later in this chapter. The Green's functions are given, therefore, in these convenient forms for both the vector and scalar potentials in the following two sections for both horizontal and vertical sources.

2.3 Vector Potential Green's Functions

For currents defined on the air-dielectric interface the vector potential Green's functions are given by [24]:

$$G_A^{xx}(\rho) = \frac{\mu_0}{2\pi}\int_0^\infty \frac{1}{D_{TE}} J_0(k_\rho \rho)\, k_\rho dk_\rho \tag{2.3.1}$$

$$G_A^{z\rho}(\rho, z_o) = \frac{\mu_0}{2\pi}\int_0^\infty \frac{\cosh(u(zo+h))}{\cosh(uh)\, D_{TE} D_{TM}} J_1(k_\rho \rho)\, k_\rho{}^2 dk_\rho \tag{2.3.2}$$

In the previous expressions, $D_{TE} = u_0 + u\coth(uh)$

$$D_{TM} = u_0\varepsilon_r + u\tanh(uh)$$

$$u = \sqrt{k_\rho^2 - k_0^2\varepsilon_r}$$

$$u_0 = \sqrt{k_\rho^2 - k_0^2}$$

Noting further that $G_A^{yy} = G_A^{xx}$

$$G_A^{yx} = G_A^{xy} = 0$$

$$G_A^{zx} = \cos\phi G_A^{z\rho}$$

$$G_A^{zy} = \sin\phi G_A^{z\rho}$$

defines the dyadic components for each of the potentials for transversely oriented currents.

When the current is vertically oriented within the substrate the vector potential Green's function is calculated from [25]:

for $-h \le z_0 \le z \le z_z \le 0$

$$G_A^{zz}(\rho, z_o, z_s) =$$

$$\frac{\mu_0}{2\pi}\int_0^{\infty} \frac{\cosh(u(z_s+h))\,(u\cosh(uz_o) - \varepsilon_r u_o \sinh(uz_o))}{u(u\sinh(uh) + \varepsilon_r u_o \cosh(uh))} J_0(k_\rho p)\, k_\rho dk_\rho \qquad (2.3.3)$$

and

for $-h \le z_s \le z \le z_o \le 0$

$$G_A^{zz}(\rho, z_o, z_s) =$$

$$\frac{\mu_0}{2\pi}\int_0^{\infty} \frac{\cosh(u(z_o+h))\,(u\cosh(uz_s) - \varepsilon_r u_o \sinh(uz_s))}{u(u\sinh(uh) + \varepsilon_r u_o \cosh(uh))} J_0(k_\rho p)\, k_\rho dk_\rho \qquad (2.3.4)$$

2.4 Scalar Potential Green's Functions

The scalar potential Green's function for sources in the air-dielectric interface are given by [24]:

$$G_V^H(\rho, z_o) = \frac{1}{2\pi\varepsilon_0}\int_0^{\infty} \frac{\sinh(u(z_o+h))N}{\sinh(uh)D_{TE}D_{TM}} J_0(k_\rho \rho)\, k_\rho dk_\rho \qquad (2.4.1)$$

where $N = u_0 + u\tanh(uh)$

When the source is vertically oreinted and imbedded in the substrate, the Green's functions are [25]:

for $-h \le z_0 \le z \le z_s \le 0$

$$G_V^V(\rho, z_o, z_s) =$$

$$\frac{1}{2\pi\varepsilon_0\varepsilon_r}\int_0^\infty \frac{\sinh(u(z_s+h))\,(u_0\varepsilon_r\cosh(uz_o) - u\sinh(uz_o))}{u(u\sinh(uh) + u_0\varepsilon_r\cosh(uh))} J_0(k_\rho\rho)\,k_\rho dk_\rho \qquad (2.4.2)$$

and for $-h \le z_s \le z \le z_o \le 0$

$$G_V^V(\rho, z_o, z_s) =$$

$$\frac{1}{2\pi\varepsilon_0\varepsilon_r}\int_0^\infty \frac{\sinh(u(z_o+h))\,(u_0\varepsilon_r\cosh(uz_s) - u\sinh(uz_s))}{u(u\sinh(uh) + u_0\varepsilon_r\cosh(uh))} J_0(k_\rho\rho)\,k_\rho dk_\rho \qquad (2.4.3)$$

2.5 Numerical Techniques for the Solution of Sommerfeld Integrals

The preceeding Green's functions represent the form of the Sommerfeld integrals best suited to calculation using a real axis integration path in the complex plane. They are a specialized form of the more general Hankel transform equations first given by Sommerfeld. The transformation from the Hankel function to the first kind Bessel function eases the calculation by reducing the infinite integral of integration to a semi-infinite

interval. Still, the numerical calculation of these integrals must be performed with great care as the Green's functions are the kernel of the MPIE and thus the critical part of the method. The semi-infinite interval is broken up into three sections as the Sommerfeld Integrals exhibit different characteristics in each of the three. The methods used for integrating the general integral

$$G = \int_0^{\infty} F(k_\rho) J_0(\rho k_\rho)\, dk_\rho \tag{2.5.1}$$

are given in the next sections.

Interval 1 $0 \le k_\rho \le k_0$

In the interval, $0 \le k_\rho \le k_0$, there exists a branch cut corresponding to the point k_0. This is due to a discontinuity in the derivative of the D_{TE} term and, while it does not cause a deformation of the path of integration, may cause a problem in trying to numerically integrate near that point. The solution is a simple change of variable. The variable of integration, k_ρ, is represented by $k_0 \cos(t)$, with t as the new variable of integration. Then $dk_\rho = -k_0 \sin(t)\, dt$ and the interval is changed from $[0, k_0]$ to $\left[\frac{\pi}{2}, 0\right]$, thus:

$$\int_0^{k_0} F(k_\rho) J_0(\rho k_\rho)\, dk_\rho \Rightarrow \int_0^{\frac{\pi}{2}} F(k_0 \cos(t)) J_0(\rho k_0 \cos(t)) k_0 \sin(t)\, dt \tag{2.5.2}$$

This integral is computed using a Gauss Legendre [26] quadrature.

Interval 2 $k_0 \le k_\rho < k_0\sqrt{\varepsilon_r}$

There will always exist at least one pole in the integrand due to the root of D_{TM}. A great simplification can be acheived if the case of only this pole existing is considered. This condition is maintained if the criteria $k_o h(\varepsilon_r - 1) < \pi/2$ is enforced. For a lossless ($Im\{\varepsilon_e\} = 0$) function this pole is on the real axis, and the pole can be found using a simple bisection scheme. When the relative permittivity is complex, however, the pole moves below the real axis and the imaginary part becomes more negative as the imaginary part of the relative permittivity becomes more significant. There is also a discontinuity in the derivative of the D_{TE} term at the point $k_\rho = k_0$ as before. The first concern is handled by extracting the pole in the integrand for the integrals which contain the D_{TM} term. A function that behaves similarly to the integrand near the pole but that is analytically integrable is subtracted from the integrand then integrated on its own and added to the final result. To find the exact location of the pole for a complex relative permittivity, a time consuming complex root finding routine would be needed, however an approximation, good for electrically thin substrates is [27]:

$$Re\{pv\} = k_0\left(1 + (k_0 h)^2 \frac{(\varepsilon_r' - 1)^2}{2\varepsilon_r'^2}\right) \tag{2.5.3}$$

$$Im\{pv\} = -(\varepsilon_r' - 1)\tan\delta\left(\frac{k_0 h}{\varepsilon_r'}\right) \tag{2.5.4}$$

Where $\varepsilon_r = \varepsilon_r'(1 - \tan\delta)$ and $\tan\delta$ is the loss tangent of the dielectric

The resulting integral can be described as shown below

$$I = (I - I_s) + I_s \tag{2.5.5}$$

Where I_s is the integral of the singular function subtracted from the integrand. A function which is assured to behave in the same manner as the integrand near the pole is derived from the residue of the integrand

$$Res = \lim_{k_\rho \to pv} F(k_\rho) J_0(\rho k_\rho)\,(k_\rho - pv) \tag{2.5.6}$$

By subtracting the function, $Res/(k_\rho - pv)$, over the entire interval, the integrand becomes regular and easy to integrate numerically. The subtracted part is then integrated analytically. After the extraction of the pole, the branch cut is handled by, once again, a change of variable. This time the variable of integration, k_ρ, is expressed as $k_0 \cosh(t)$. With this change, dk_ρ becomes $k_0 \sinh(t)\,dt$ and the interval is transformed from $[k_0, k_0\sqrt{\varepsilon_r}]$ to $[0, \operatorname{acosh}(\sqrt{\varepsilon_r})]$. Thus

$$\int_{k_0}^{k_0\sqrt{\varepsilon_r}} F(k_\rho) J_0(\rho k_\rho)\,dk_\rho \Rightarrow$$

$$\int_0^{\operatorname{acosh}\sqrt{\varepsilon_r}} \left(F(\rho k_0 \cos(t)) J_0(\rho k_0 \cos(t)) - \frac{Res}{(k_0 \cosh(t) - pv)} \right) k_0 \sinh(t)\,dt$$

$$+ \int_{k_0}^{k_0\sqrt{\varepsilon_r}} \frac{Res}{(k_\rho - pv)} dk_\rho \,. \tag{2.5.7}$$

The last part is analytically integrated by

$$\int_{k_0}^{k_0\sqrt{\varepsilon_r}} \frac{Res}{(k_\rho - pv)} dk_\rho = \frac{Res}{2} \ln\left(\frac{\left(k_0\sqrt{\varepsilon_r} - Re\{pv\}\right)^2 + (Im\{pv\})^2}{(Re\{pv\} - k_0)^2 + (Im\{pv\})^2} \right)$$

$$+ jRes\left(\operatorname{atan}\left(\frac{k_0\sqrt{\varepsilon_r} - Re\{pv\}}{Im\{pv\}} \right) + \operatorname{atan}\left(\frac{Re\{pv\} - k_0}{Imp\{pv\}} \right) \right) \tag{2.5.8}$$

Interval 3 $k_0\sqrt{\varepsilon_r} \le k_\rho < \infty$

In the final interval, the integrands oscillate as the corresponding Bessel function. Since this part of the integral is the dominant part in the near field region, it is extremely important that special care be taken in its evaluation. A nonlinear transformation was first studied based on Shanks method [28]. This method provided no easy way to automatically check for the relative error in the terms and a new algorithm was sought. A special technique was then developed, based on the method of averages [24]. The method of averages is applied to integrals of the form:

$$I = \int_a^\infty f(x)\, g(x)\, dx \tag{2.5.9}$$

where f is an oscillating function of x and g is a function that converges monotonically to zero. If the oscillatory part is approximately periodic, as the Bessel function for example, then the integral can be represented by the sum of integrals over each half-period as

$$I = \int_a^{\alpha_1} f(x)\, g(x)\, dx + \lim_{n \to \infty} I_n^1 \tag{2.5.10}$$

where $I_n^1 = \sum_{i=1}^{n} I_i^0$ and $I_i^0 = \int_{\alpha_i}^{\alpha_{i+1}} f(x)\, g(x)\, dx$

Where α_i are the zeroes of the oscillating function *f(x)*. When the function *g(x)* converges monotonically, the successive terms of the series I_n^1 alternately overestimate and underestimate the value of the integral. Taking the average of any two successive terms of this series, therefore, serves as a first order approximation to the value of the integral. The terms in the series of these averages is given by

$$I_n^2 = \frac{I_n^1 + I_{n+1}^1}{2} \tag{2.5.11}$$

Using this method, it is recognized that once again the series represented by I_n^2 also alternately overestimates and underestimates the value of the integral (the value of the limit of the infinite series). By taking the averages once again, a better approximation of the sum is found. This procedure is repeated until an acceptable level of error between estimates is obtained.

The method of averages is only part of the algorithm used here. In some of the Sommerfeld integrals the integrands decay effectively to zero before any significant oscillation occurs. The effect is noticed when the source and observation points do not have the same z values, and the hyperbolic functions in the integrand dominate. In this case the method of averages will be less accurate than a simple truncation of the integral. Hence, the method is also required to recognize when the hyperbolic functions dominate and and a

simple numerical integration over a truncated interval is required. Furthermore, the appropriate truncated interval must be obtained

The algorithm developed here calculates the approximate value of the variable of integration, x, for an integrand approaching zero, this is denoted x'. If the value of x' is less than the first root of the integrand, corresponding to the oscillating function, a simple truncated integration is performed in the interval $[a, x']$.

$$I = \int_{a}^{x'} f(x)\, g(x)\, dx \tag{2.5.12}$$

Other wise the method of averages is implemented. There are, however, some cases where the integrand decays to zero but not within the first half period, or cases when the integral converges faster that the method of averages will. This situation, then, is also introduced into the algorithm. After calculating the value of the integral over each half-period as it is required, a decision is made. If the value of the integral over the most recent half-period is less than 0.1% of the value of the integral over the previous half-period then the averaging is terminated and the value of the summed series up to that point is used. Otherwise the method of averages is continued, and the algorithm is repeated using an exit criteria of 0.1% for the difference in consecutive averages. The total algorithm is best illustrated by a flow-chart (figure 2.5.1).

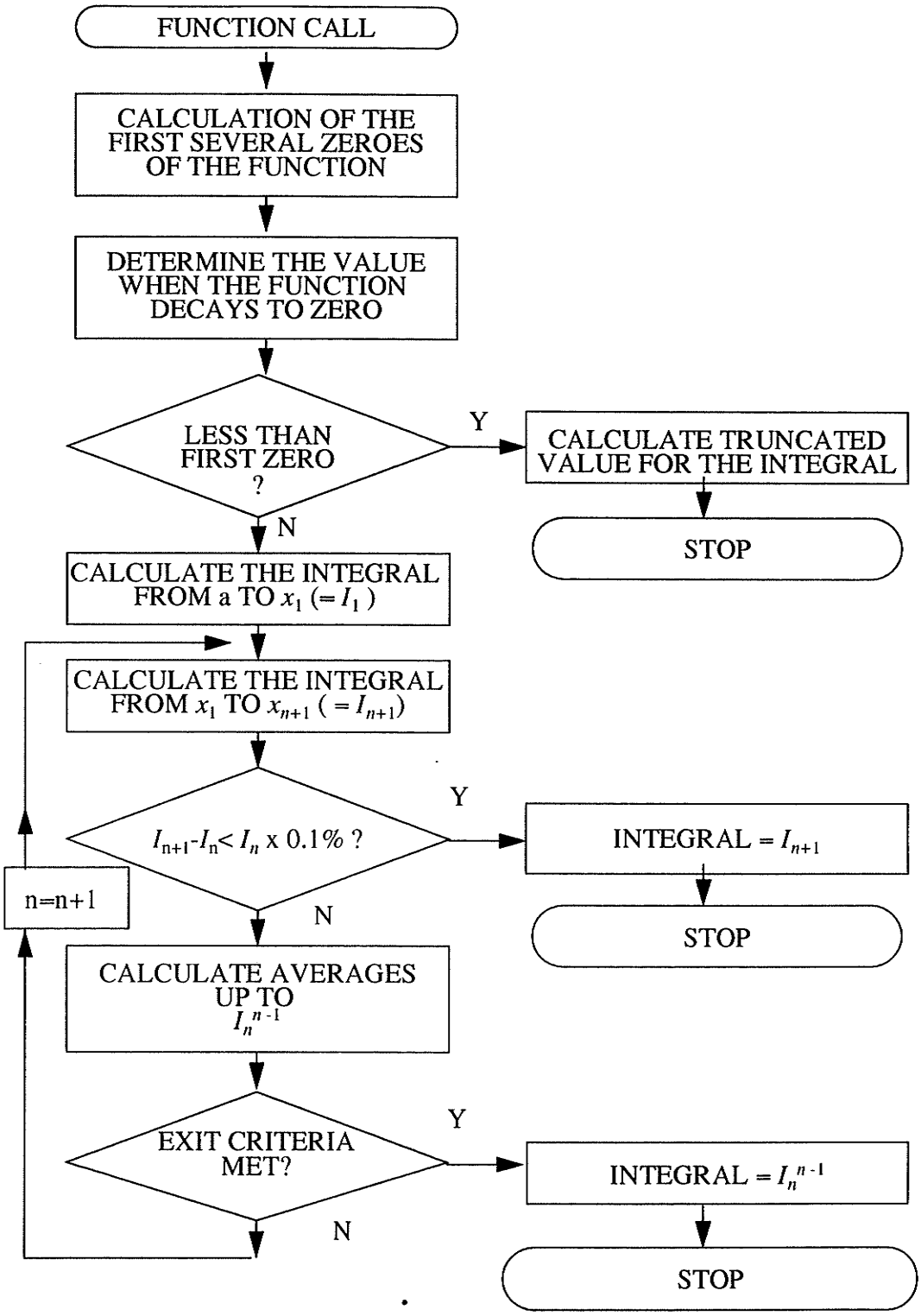

Fig. 2.5.1 Flow Chart Representing the Calculation of Oscillating Integrals

3 Moments Method Solution of the MPIE

3.1 Overview

The Method of Moments (MoM) can be applied to equations of the form [18]:

$$L(\xi) = \varsigma \tag{3.1.1}$$

Where L is a linear operator on the unknown response, ξ, and ς is the known excitation.

In the application of the MoM to equation (3.1.1), the unknown response is expanded over a set of basis functions in the domain of L as:

$$\xi = \sum_n a_n \xi_n \tag{3.1.2}$$

Here, a_n are the amplitudes of each basis function, ξ_n.

A set of testing functions ($w_1, w_2, w_3,...$) are then defined in the range of L along with an inner product, $\langle f, g \rangle$, which satisfies the following:

$$\langle f, g \rangle = \langle g, f \rangle$$

$$\langle \alpha f + \beta g, h \rangle = \alpha \langle f, h \rangle + \beta \langle g, h \rangle \tag{3.1.3}$$

$$\begin{aligned} \langle f^*, f \rangle &> 0 \qquad \text{if } f \neq 0 \\ &= 0 \qquad \text{if } f = 0 \end{aligned}$$

The application of the testing function through the inner product, as defined above, leads to a linear expression of equation (3.1.1):

$$\sum_n a_n \langle L(\xi_n), w_m \rangle = \langle \varsigma, w_m \rangle \tag{3.1.4}$$

Some care must be taken in the selection of the basis and testing functions. First, the set of basis functions must be capable of a reasonable approximation of the unknown response. Clearly, the number of terms taken in the summation is related to the accuracy of the obtained solution. Another consideration is the ease in which the operator L is applied to the basis functions, x_n. Finally, as the testing function is required in order to enforce the equality of equation (3.1.1) it is necessary that it is of a similar order as the basis functions so that the computational effort expended in applying the basis functions is not wasted in the testing.

3.2 Basis Functions for Surface Conductors

Segmentation of the Conducting Surface

In applying the MoM to solve for the currents on the surface conductor, the arbitrary shapes of the conductors are replaced by groups of rectangular cells, which will henceforth be called charge cells, as shown in figure 3.2.1. The boundary of the conductor, then, is approximated as closely as possible by a "Manhattan" type boundary where curves are replaced by series of straight line segments. To simplify some of the resulting calculations, all charge cells are all taken to be of the same dimensions, $(\Delta x, \Delta y)$. A scheme where different sized charge cells may be used, but this scheme would involve much more complicated programming and could not take advantage to the time saving techniques introduced later in this chapter.

Some definitions are made here in order to clarify the description of the basis functions. The current is approximated, as described in the next section, by overlapping basis functions. Each current basis function is defined over a current cell which consists of two adjacent charge cells whose interface is perpendicular to the direction of the current as shown in figure 3.2.2. An arbitrary x-directed current cell, whose centre is designated as r_{xi} will be given the label S_i, the corresponding charge cells are S_i^- and S_i^+. The centres of the two charge cells, $\hat{r}_{xi}^-$ and $\hat{r}_{xi}^+$ respectively, are connected by a test segment C_{xi}. The overlapping cells and corresponding test segments occur in both the x and y directions, hence a charge cell may belong to a maximum of four different current cells and its centre may be a terminus for up to four test segments. A similar notation is used for y-directed current cells.

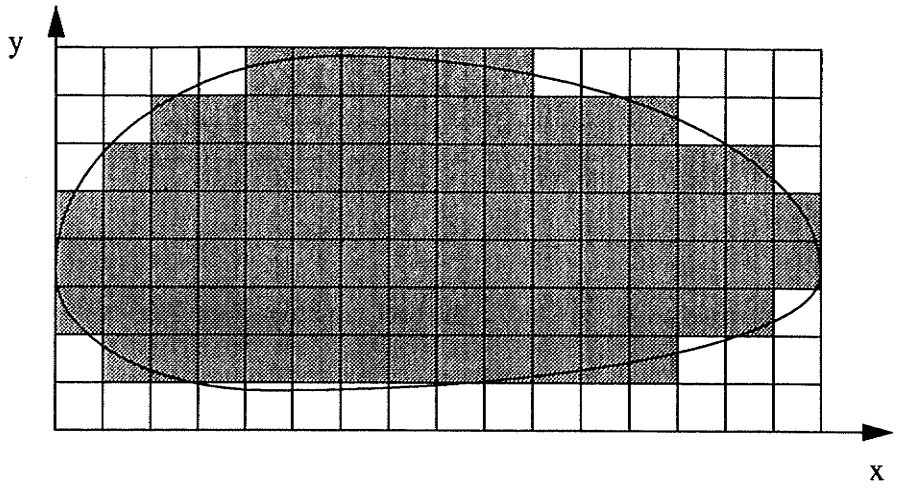

Fig. 3.2.1 Segmentation of an Arbitrary Shaped Conducting Surface

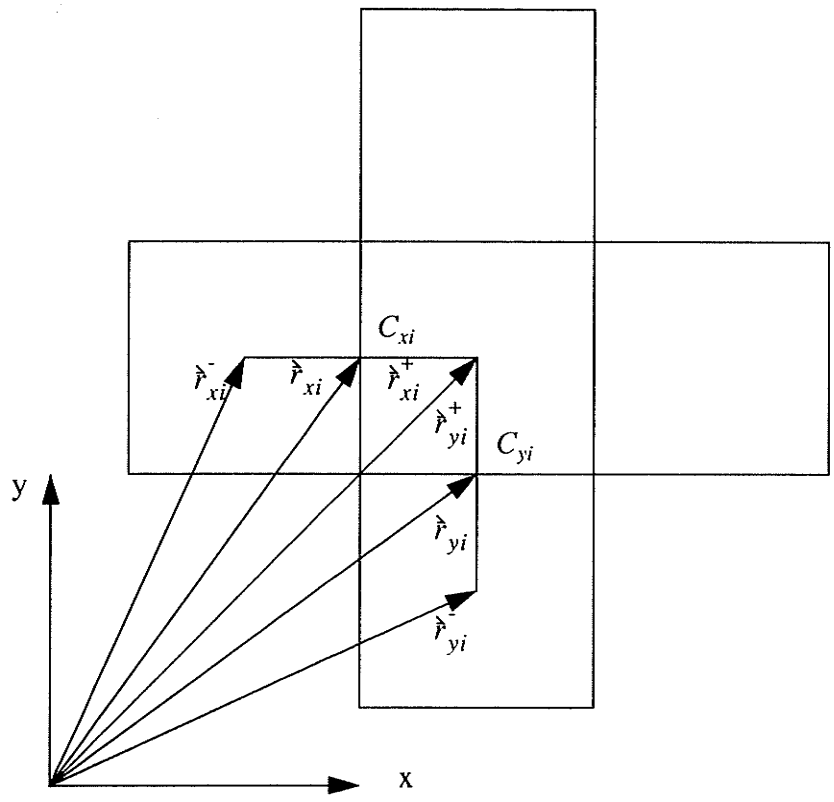

Fig. 3.2.2 Specifications for the Current and Charge Segments

Current Basis Functions

As previously stated, the main goals in selecting a basis function are first to ensure that the basis function is capable of a reasonable approximation of the unknown response (the current) and secondly to ensure the application of the linear operator to it results in a relatively simple solution scheme. A further consideration here is that a basis function for the surface charge is also required and that these charge basis functions are related to the gradient of the current basis functions. Therefore the derivative of the current basis functions are also required, and must be relatively simple to derive. With this in mind, the basis functions for the current are chosen to be overlapping triangular roof-top functions as in [19], shown in figure 3.2.3 A and expressed mathematically, for x directed current cells centred at (x_i, y_i), and y directed current cells centred at (x_j, y_j) by:

$$T_{xi}(\hat{r}) = 1 - \frac{|x - x_i|}{\Delta x} \tag{3.2.1}$$

for

$$|x - x_i| \le \Delta x \quad \text{and} \quad |y - y_i| \le \frac{\Delta y}{2}$$

and

$$T_{yj}(\hat{r}) = 1 - \frac{|y - y_j|}{\Delta y} \tag{3.2.2}$$

for

$$|y - y_j| \le \Delta y \quad \text{and} \quad |x - x_j| \le \frac{\Delta x}{2}$$

Where Δx and Δy are the dimensions of a charge cell as previously defined. It then follows that the current distribution in the x and y directions are approximated by the two summations

$$J_{sx} = \frac{1}{\Delta y} \sum_{i=1}^{Nx} I_{xi} T_{xi} \tag{3.2.3}$$

and

$$J_{sy} = \frac{1}{\Delta x} \sum_{j=1}^{Ny} I_{yj} T_{yj} \tag{3.2.4}$$

Dividing by $\frac{1}{\Delta x}$ and $\frac{1}{\Delta y}$ in these equations ensures that definition of a current density is preserved.

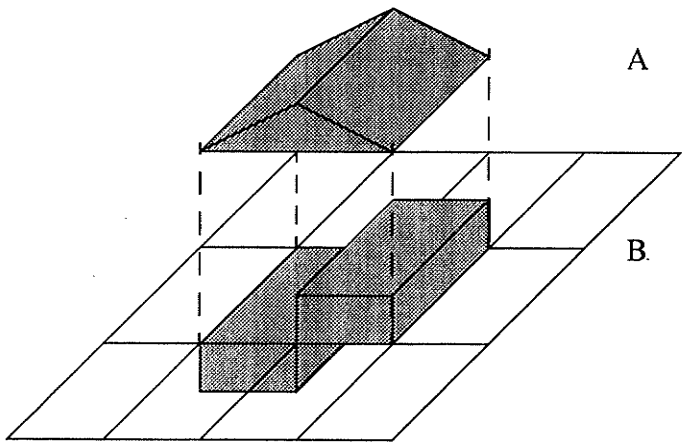

Fig. 3.2.3 Basis Functions for the Surface Current (A) and Charge (B)

Charge Basis Functions

The basis functions approximating the surface charge density follow easily by the application of the continuity equation (3.2.5) to the current basis functions

$$\nabla \cdot \hat{\mathbf{J}}_s + j\omega\rho_s = 0 \tag{3.2.5}$$

Through this, then, the charge basis functions are given as rectangular pulse functions with unit magnitude defined over each half of a current cell as shown in figure 3.2.3 B.

$$\Pi(\hat{r}_i) = 1 \tag{3.2.6}$$

for $|x - x_i| \le \frac{\Delta x}{2}$ and $|y - y_i| \le \frac{\Delta y}{2}$.

The charge distribution on the surface conductor as approximated by these basis functions is given by the series

$$\rho_s = \frac{1}{j\omega\Delta x\Delta y}\left[\sum_{i=1}^{Nx} I_{xi}\left(\Pi\left(\hat{r}_i^{+}\right) - \Pi\left(\hat{r}_i^{-}\right)\right) + \sum_{j=1}^{Ny} I_{yj}\left(\Pi\left(\hat{r}_j^{+}\right) + \Pi\left(\hat{r}_j^{-}\right)\right)\right] \tag{3.2.7}$$

3.3 Basis Functions for Vertical Wire Components

Segmentation of Wire Components

The overlapping basis function approximation of the current is used with the wire sections in a manner similar to that of the surface conductors. Thus, the wires are segmented similarly to the conducting surface. As shown in figure 3.3.1 the wire is divided up into charge cells of equal height, Δz. Two charge cells with centres z_i^+ and z_i^- respectively comprise one current cell which is centred at z_i. A test segment C_{zi} connects the centres of the two charge cells in a manner analogous to the surface test segments.

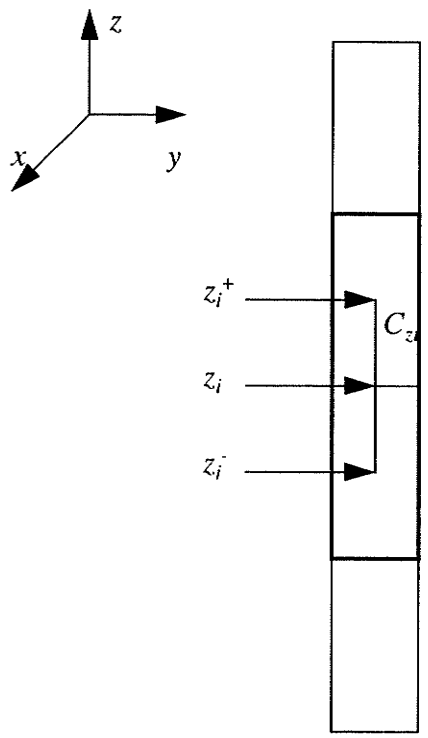

Fig. 3.3.1 Segmentation of Wire Components

Current Basis Functions

The current basis function chosen here should be analogous to the surface current basis functions to maintain homogeneity in the numerical solution and is thus chosen to be, once again, a triangular function. The total current in a wire segment is I_{zi}. At the frequencies that we are interested in, the current can be assumed to exist totally on the surface of the conductor by the skin effect. Since there should be no variation of the in the angular direction, that surface current density is the total current in the wire divided by the circumference of the wire. Applying the triangular function to the current density in the wire gives the current basis function for a current cell centred at z_i as shown in figure 3.3.2

$$T_{zi} = 1 - \frac{|z - z_i|}{\Delta z} \tag{3.3.1}$$

For $|z - z_i| \leq \Delta z$

At the point where the wire touches the ground plane, this function description must be altered. Since the current exists above the ground plane but not below, the basis function for this current is simply the same triangle function with the same properties except that it is only defined on one charge cell, directly above the ground plane as shown in figure 3.3.2

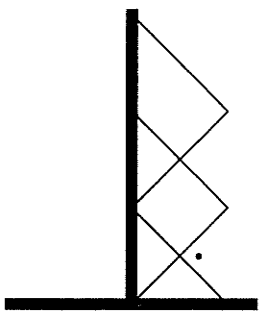

Fig. 3.3.2 Current Basis Functions Over the Wire Elements

It then follows that the currents in the z-direction will be approximated by the summation:

$$J_{sz} = \frac{1}{2\pi r_c} \sum_{i=1}^{Nz} I_{zi} T_{zi} \tag{3.3.2}$$

where r_c is the radius of the conducting pin.

Charge Basis Functions

Once again by application of the continuity equation (3.2.5) to the current basis functions the charge density basis functions are determined to be unit magnitude rectangular pulses defined over the charge cells.

$$\Pi(z_i) = 1 \tag{3.3.3}$$

For $|z - z_i| \leq \frac{\Delta z}{2}$

The charge distribution over the wire components is therefore approximated by the summation:

$$\rho_s = \frac{1}{j\omega 2\pi r_c \Delta z} \sum_{i=1}^{Nz} I_{zi} \left(\Pi\left(z_i^+\right) - \Pi\left(z_i^-\right) \right) \quad . \tag{3.3.4}$$

3.4 Treatment of Junctions Where Wires Meet Surface Conductors

Current Across a Junction

At the point where a wire contacts the microstrip surface, a special function must be defined to convert the z-directed currents on the wire to planar currents on the surface and vice-versa. This function must follow three specific criteria. First, the current must be continuous at the contact point. All current in the z-direction must be converted into current in the x and y directions. The current must also spread evenly away from the contact point in each direction, at least locally. Finally the function must decay to zero at some distance from the contact point that is comparable to the segmentation of the microstrip surface. A simple model for the current on the surface local to the junction is used here which fits very well with the use of the rooftop basis functions. The current enters the surface through a half triangle function similar to that used for a wire close to the ground plane in the previous section. The current enters through the point of contact and spreads equally in each direction as shown in figure3.4.1. at the junction point $(x_j, y_j, 0)$ this is mathematically described by

$$J_{jun} = J_{wj}\hat{z} + J_{pjx}\hat{x} + J_{pjy}\hat{y} \tag{3.4.1}$$

Where:

$$J_{wj} = \frac{1}{2\pi r_c} I_j \left(1 - \frac{|z|}{\Delta z} \right) \tag{3.4.2}$$

For $|z| \leq \Delta z$

$$J_{pjx} = \frac{1}{4\Delta y} sign\,(x - x_j)\, I_j \left(1 - \frac{|x - x_j|}{2\Delta x} \right) \tag{3.4.3}$$

$$J_{pjy} = \frac{1}{4\Delta x} sign\,(y - y_j)\, I_j \left(1 - \frac{|y - y_j|}{2\Delta y} \right) \tag{3.4.4}$$

For $|x - x_j| \leq \frac{\Delta x}{2}$ and $|y - y| \leq \frac{\Delta y}{2}$

We note here that the total z-directed current at the junction is equal to I_j and that on the surface, the total current is $4\left(\frac{1}{4} I_j\right) = I_j$

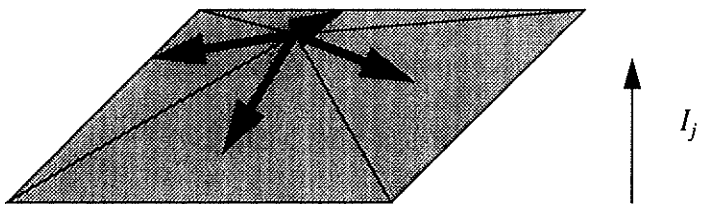

Fig. 3.4.1 Description of the Current at Junction

Charges at a Junction

The charge basis functions are once again found by applying the continuity equation (3.2.5) to the different currents found in the description of the junction. It should be noted here that while the basis functions describing the current are discontinuous at the junction point, it has been ensured that the current itself is continuous and any effects of the discontinuous parts cancel each other. With this in mind then, the charges at the junction are described by a single two dimensional pulse over the charge cell on the surface conductor and a z-directed pulse function over the charge cell adjacent to the surface, on the wire.

$$\rho_s = \frac{I_j}{j\omega}\left[\frac{1}{\Delta x \Delta y}\Pi(\grave{r}_j) - \frac{1}{\Delta z 2\pi r_c}\Pi(z_j)\right] \tag{3.4.5}$$

3.5 Testing Functions

In selecting of a proper testing function the main requirement is that the level of accuracy aimed for in the choice of the basis functions is not compromised. For instance, it is not reasonable to define complicated two dimensional basis functions over the entire surface of the conductor and then test with a Dirac-delta weighting function essentially enforcing the equality at only a fixed number of points. However, once again the simplicity of applying the functions and time needed for computations must also be considered. A Galerkin method may be used, in essence using the same function for testing as is used for the basis function. This method may become computationally expensive due to the

complexity involved. The choice made here is the use of unidimesional pulse functions, also called razor functions. For the surface conductor and the wire, the razor functions are defined from the centre of a charge cell to the centre of the adjacent charge cell as shown in figure 3.5.1. Testing with these functions ensures that the boundary condition is enforced on straight line segments on the conductors, but requires less computation than the Galerkin method. In fact it is a compromise between accuracy and efficiency.

In the case of the current segment adjacent to the ground plane, only one charge cell corresponds to the segment and therefore the testing segment is truncated at the ground plane as shown in figure 3.5.1. A testing function corresponding to the junctions must also be defined so that the number of unknown current coefficients does not exceed the number of equations. In the same way as the current cell beside the ground plane, the testing function for the junction is defined by a razor function joining the contact point of the wire with the microstrip surface and the centre of the charge cell just below the surface. Previous works [37] have included segments on the surface near the junction as part of this test function, but that is considered here to be somewhat complicated and unnecessary as the testing already performed on the surface makes this testing redundant

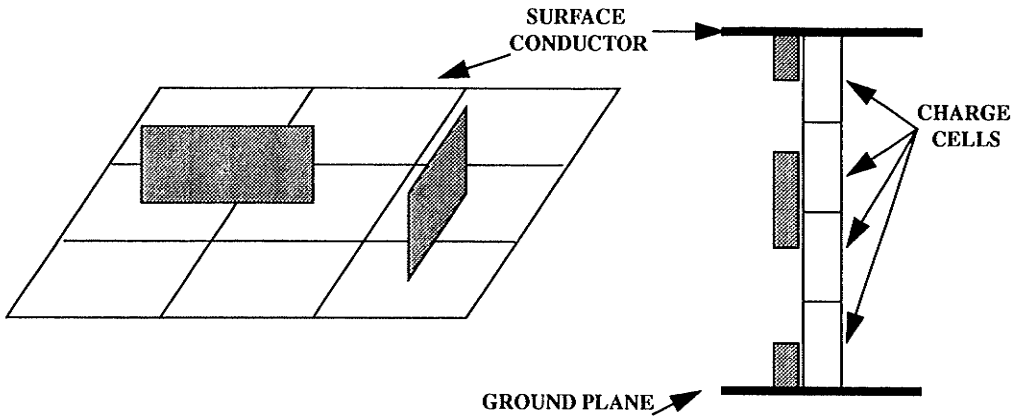

Fig. 3.5.1 Razor Testing Functions Across the Conductors

The testing function is implemented through the definition of the inner product, here the inner product is the integral operation of equation (3.5.1) over the entire surface of the structure. Integration is the definition of the inner product used in most MoM applications.

$$\langle w(x), g(x) \rangle = \int_S g(x)\, w(x)\, dx \qquad (3.5.1)$$

Using this definition, and the previously defined testing functions, the effect of imposing the testing on the MPIE is to integrate the function along a series of finite line segments defined over all conductors in the given structure.

3.6 Discrete Green's Functions

Discrete Scalar Potential Green's Function

The notation and computation of the moment matrix is simplified through the use of discrete Green's Functions. For the scalar potential, the discrete Green's functions are the superposition integrals of the basis function for the charge distribution over one charge cell with the scalar Green's function for sources on that charge cell given an observation point. We additionally multiply by a factor of $2\pi\varepsilon_o$ to ease the notation later. This factor will later be divided out again

For charges associated with the surface elements

$$\Gamma_V^H(i,j) = \frac{2\pi\varepsilon_0}{\Delta x\Delta y}\int_{S_j}\int G_V^H(\vec{r}_i, z_i|\vec{r}_j, 0)\cdot\Pi(\vec{r}_j)\,dS_j \tag{3.6.1}$$

For charges associated with the vertical elements, the charge is spread evenly around the circumference of the wire. When the source and observation points have the same x and y components, or when the distance between source and observation points is very large, the angular distribution of the charge has a negligible effect or no effect, on the integration. In this case the discrete Green's function is obtained only by integrating in the z-direction and multiplying by the circumference, $2\pi r_c$. Then

$$\Gamma_V^V(i,j) = \frac{2\pi\varepsilon_0}{\Delta z}\int_{z_j-\frac{\Delta z}{2}}^{z_j+\frac{\Delta z}{2}} G_V^V(\vec{r}_i, z_i|\vec{r}_j, z_j)\cdot\Pi(z_j)\,dz_j \tag{3.6.2}$$

When the distance between the source and observation points is small but not zero, however, the radius of the wire is a considerable part of the distance between source and observation points and is not negligible. In this case, the discrete Green's function is calculated using the double integral

$$\Gamma_V^V(i,j) = \frac{2\pi\varepsilon_0}{2\pi r_c \Delta z}\int_0^{2\pi}\int_{z_j-\frac{\Delta z}{2}}^{z_j+\frac{\Delta z}{2}} G_V^V(\hat{r}_i, z_i|(\hat{r}_j, z_j)) \cdot \Pi(z_j)\, dz_j d\theta \tag{3.6.3}$$

Discrete Vector Potential Green's Functions

The discrete vector potential Green's functions are defined in a similar manner as those of their scalar counterparts except that the integration is performed over a current cell and the rooftop basis functions are used as the source. In this case the function is multiplied by a factor of $2\pi/\mu_0$ here to ease the notation later.

$$\Gamma_A^{xx}(\hat{r}|\hat{r}_n') = \frac{2\pi}{\mu_0 \Delta y}\int\int_{S_n} G_A^{xx}(\hat{r}|\hat{r}') \cdot T_{xn}(r')\, dS' \tag{3.6.4}$$

$$\Gamma_A^{zx}(\hat{r}|\hat{r}_n') = \frac{2\pi}{\mu_0 \Delta y}\int\int_{S_n} G_A^{zx}(\hat{r}|\hat{r}') \cdot T_{xn}(r')\, dS' \tag{3.6.5}$$

Similar expressions for Γ_A^{yy} and Γ_A^{yz} are obtained by exchanging y for x and vice versa in the above equations.

When the surface current describes the current at a junction, the discrete Green's function is found in a similar manner with the exception that the integration is taken over a single charge cell and the basis function is that of the junction function as written in equation (3.2.3) or (3.2.4). This results in the form:

$$\Gamma_A^{xj}(\hat{r}|\hat{r}_n') = \frac{2\pi}{\mu_0 4\Delta y}\int\int_{S_n} G_A^{xx}(\hat{r}|\hat{r}') \cdot \left(sign(x-x_n')\left(1-\frac{|x-x_n'|}{2\Delta x}\right)\right)dS' \qquad (3.6.6)$$

Where, once again the expression for Γ_A^{yj} is obtained by exchanging y and x in the previous expression. When the effect of the junction in the z direction is desired, the discrete Green's function is:

$$\Gamma_A^{zj}(\hat{r}|\hat{r}_n') =$$

$$\frac{2\pi}{\mu_0 4\Delta y}\int\int_{S_n} G_A^{zx}(\hat{r}|\hat{r}') \cdot \left(sign(x-x_n')\left(1-\frac{|x-x_n'|}{2\Delta x}\right)\right)dS' +$$

$$\frac{2\pi}{\mu_0 4\Delta x}\int\int_{S_n} G_A^{zy}(\hat{r}|\hat{r}') \cdot \left(sign(y-y_n')\left(1-\frac{|y-y_n'|}{2\Delta y}\right)\right)dS' \qquad (3.6.7)$$

The discrete Green's function for vertical currents are obtained by integrating over the current cell on the wires.

$$\Gamma_A^{zz}(\hat{r}|\hat{r}_n') = \frac{2\pi}{\mu_0 2\pi r_c}\int\int_{S_n} G_A^{zz}(\hat{r}|\hat{r}') \cdot T_{zn}(r')\,dS' \qquad (3.6.8)$$

The Green's functions are, by definition, singular when the source and observation points coincide. Therefore, when the discrete Green's functions are to be calculated for source and observation points in the same cell, numerical techniques alone will not be able to accurately compute the surface integral.

When the cell is on a wire section the singularity is easily avoided by applying the testing of the field to the centre of the wire. Since, because of the skin effect at high frequencies, the current will exist mainly on the outer circumference of the wire, the source and observation points will never coincide.

In the case where the cell is on the surface conductor, the singularity corresponding to a zero separation distance must first be extracted. Fortunately, this singularity is very closely associated with the inverse of the distance of separation, for both the vector and scalar potential Green's functions. The function obtained after extracting the singular part will be regular and easy to integrate using numerical techniques. The extracted function can then be integrated analytically and added back to the result. For the vector and scalar potentials, the singular part is determined by considering the Green's function for the static (f=0) case. It will then follow that $k_0 = 0$, and by substituting this into the expressions for the Green's functions;

$$G_V^{\text{sing}} = \frac{1}{2\rho\,(\varepsilon_r + 1)} \tag{3.6.9}$$

$$G_A^{\text{sing}} = \frac{1}{2\mu\rho} \tag{3.6.10}$$

This singular part is then integrated over the charge and current cells using the following two equations [29]:

$$\iint \frac{1}{\sqrt{x^2+y^2}} dydx = x\log(y+R) + y\log(x+R) \tag{3.6.11}$$

$$\iint \frac{x}{\sqrt{x^2+y^2}} dydx = \frac{1}{2}yR + x^2\log(y+R) \tag{3.6.12}$$

where necessary.

3.7 Generating and Solving the Matrix Equation

All that remains, then, is to approximate the appropriate potential is to sum up the discrete Green's Functions scaled by the basis function coefficients over the entire structure. That is

$$\frac{\mu_0}{2\pi}\vec{\mathbf{A}}(\hat{r}) = \sum_{n=1}^{Nx} I_{xn}\left(\hat{x}\Gamma_A^{xx}(\hat{r}|\hat{r}_n) + \hat{z}\Gamma_A^{zx}(\hat{r}|\hat{r}_n)\right) + \sum_{m=1}^{Ny} I_{ym}\left(\hat{y}\Gamma_A^{yy}(\hat{r}|\hat{r}_m) + \hat{z}\Gamma_A^{zy}(\hat{r}|\hat{r}_m)\right)$$

$$+ \sum_{l=1}^{Nz} \hat{z} I_{zl}\Gamma_A^{zz}(\hat{r}|\hat{r}_l) + \sum_{k=1}^{Nj} I_{jk}\left(\hat{x}\Gamma_A^{xj}(\hat{r}|\hat{r}_k) + \hat{y}\Gamma_A^{yj}(\hat{r}|\hat{r}_k) + \hat{z}\Gamma_A^{zj}(\hat{r}|\hat{r}_k)\right) \tag{3.7.1}$$

and

$$\frac{j\omega}{2\pi\varepsilon_0}V(\hat{r}) = \sum_{n=1}^{Nx} I_{xn}\left(\Gamma_V^H\left(\hat{r}|\hat{r}_n^+\right) - \Gamma_V^H\left(\hat{r}|\hat{r}_n^-\right)\right) + \sum_{m=1}^{Ny} I_{ym}\left(\Gamma_V^H\left(\hat{r}|\hat{r}_m^+\right) - \Gamma_V^H\left(\hat{r}|\hat{r}_m^-\right)\right)$$

$$+ \sum_{l=1}^{Nz} I_{zl}\left(\Gamma_V^V\left(\hat{r}|\hat{r}_l^+\right) - \Gamma_V^V\left(\hat{r}|\hat{r}_l^-\right)\right) + \sum_{k=1}^{Nj} I_{jk}\left(\Gamma_V^H\left(\hat{r}|\hat{r}_k^+\right) - \Gamma_V^V\left(\hat{r}|\hat{r}_k^-\right)\right) \tag{3.7.2}$$

In the preceding equations, Nx, Ny, Nz, and Nj are the number of current cells in the x, y, and z directions and the number of junctions respectively. The $I_{\varsigma i}$ are the coefficients representing the ith current basis function in the ς direction. Recalling equation 2.1.4.

$$\vec{\mathbf{E}}^{s}(\vec{r}) = -j\omega\vec{\mathbf{A}}(\vec{r}) - \nabla V(\vec{r}) \tag{3.7.3}$$

The application of the testing function to this is equivalent to taking a line integral over each of the test segments. For the three directions

$$\int_{Cxi} E_x^s(\vec{r})\,dx = -j\omega \int_{Cxi} A_x(\vec{r})\,dx - \left(V\left(\vec{r}_{xi}^{+}\right) - V\left(\vec{r}_{xi}^{-}\right)\right) \tag{3.7.4}$$

$$\int_{Cyj} E_y^s(\vec{r})\,dy = -j\omega \int_{Cyj} A_y(\vec{r})\,dy - \left(V\left(\vec{r}_{yj}^{+}\right) - V\left(\vec{r}_{yj}^{-}\right)\right) \tag{3.7.5}$$

$$\int_{Czk} E_z^s(\vec{r})\,dz = -j\omega \int_{Czk} A_z(\vec{r})\,dz - \left(V\left(\vec{r}_{zk}^{+}\right) - V\left(\vec{r}_{zk}^{-}\right)\right) \tag{3.7.6}$$

Replacing the scattered field by these expressions in the MPIE, a matrix equation is obtained of the form:

$$[Z]\,[I] = \frac{Z_0}{2\pi}[V] \tag{3.7.7}$$

The form of the Z matrix depends on the type of feed and load conditions which are described in detail in the next chapter, and is solved using a simple Gaussian elimination

technique.Similarly, the form of the excitation vector is dependent on the type of feed and is also detailed in the following chapter

3.8 Techniques to Improve Computation Speed

The discrete Green's functions for both the scalar and vector potentials in a given structure and at a given frequency are only dependent on the separation distance between source and observer cells and the size of the current or charge cells themselves. Since, in segmenting the surface conductors and wire components, a uniform size was used throughout, some symmetry effects may be used to enhance the speed of calculating the discrete Green's functions. When one discrete scalar Green's function is calculated for a given source-observation separation distance then, this can be used for all elements with the same source-observer separation distance as shown in figure 3.8.1. Here, then

$$\Gamma_V^H(i,j) = \Gamma_V^H(j,k)$$

For the vector potential, once a calculation is made for the discrete Green's function, all elements which have the same distance of separation between both charge cells comprising the source and observation cells as shown in figure 3.8.1 are then known.

$$\Gamma_A^{xx}(l,m) = \Gamma_A^{xx}(m,n)$$

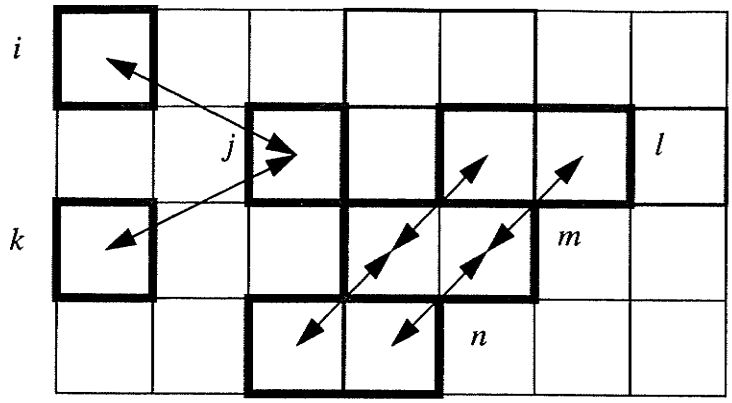

Fig. 3.8.1 Symmetry in the Discrete Green's Functions

In addition to this, as the variation in both the scalar and vector Green's functions are very strong only in the region where the source and observation points are very close, some approximations may be made when separations are large. Figure 3.8.2 shows the real and imaginary parts of the scalar Green's function for source and observation points on the air-dielectric interface as a function of the distance in wavelengths. It is plainly shown here that at a separation of one quarter wavelength, the Green's Function is well out of the region where the strongest variations occur. A similar characteristic is found for the vector potential. Therefore one quarter wavelength is chosen as the threshold for using the aforementioned approximation.

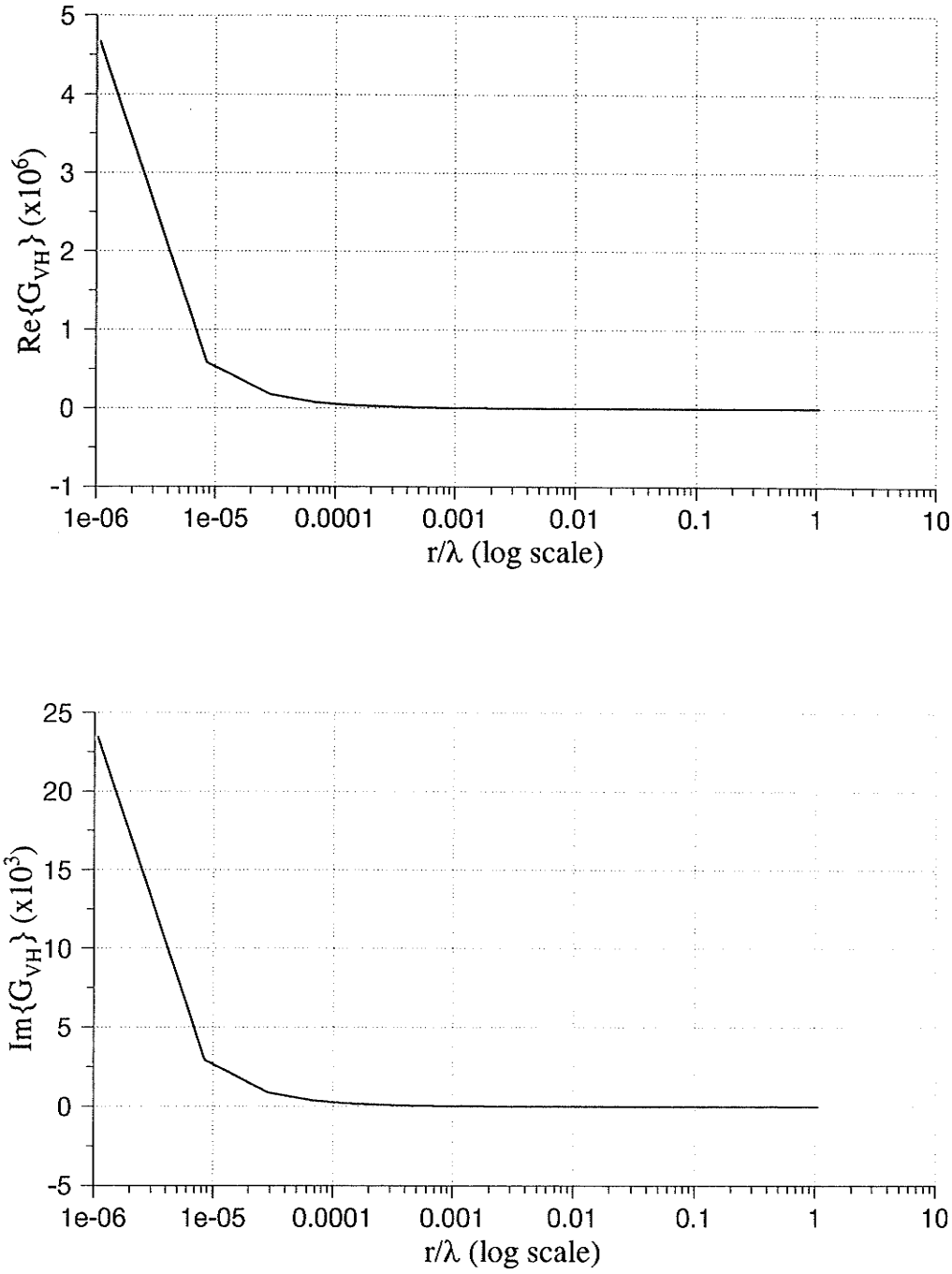

Fig. 3.8.2 Real and Imaginary Parts of the Scalar Potential Green's Function as a Function of Source - Observation Point Separation Distance

The approximation for the discrete scalar Green's function is obtained by assuming that the Green's function itself is constant over the surface of the charge function that it is integrated over. That is, for the scalar potential:

$$\int\int_{S_j} G_V^H(\hat{r}_i, z_i|\hat{r}_j, 0) \cdot \Pi(\hat{r}_j)\, dS_j = G_V^H(\hat{r}_i, z_i|\hat{r}_j, 0)\,\Delta x\Delta y \tag{3.8.1}$$

and

$$\int_{z_j-\frac{\Delta z}{2}}^{z_j+\frac{\Delta z}{2}} G_V^V(\hat{r}_i, z_i|\hat{r}_j, z_j) \cdot \Pi(z_j)\, dz_j = G_V^V(\hat{r}_i, z_i|\hat{r}_j, z_j)\,\Delta z \tag{3.8.2}$$

Similarly, for the discrete vector potential Green's functions

$$\frac{1}{\Delta y}\int\int_{S_n} G_A^{xx}(\hat{r}|(\hat{r}')) \cdot T_{xn}(r')\, dS' = G_A^{xx}(\hat{r}|(\hat{r}'))\,\Delta x \tag{3.8.3}$$

$$\frac{1}{4\Delta y}\left(\int\int_{S_n} G_A^{xx}(\hat{r}|(\hat{r}')) \cdot \left(sign(x-x_n')\left(1-\frac{|x-x_n'|}{2\Delta x}\right)\right)dS'\right) = 0 \tag{3.8.4}$$

$$\frac{1}{\Delta y}\int\int_{S_n} G_A^{zx}\hat{r}|(\hat{r}') \cdot T_{xn}(r')\, dS' = G_A^{z\rho}\hat{r}|(\hat{r}')\,(\cos\phi)\,\Delta x \tag{3.8.5}$$

and

$$\frac{1}{2\pi r_{wire}}\int\int_{S_n} G_A^{zz}(\hat{r}|(\hat{r}')) \cdot T_{zn}(r')\, dS' = G_A^{zz}(\hat{r}|(\hat{r}'))\,\Delta z \tag{3.8.6}$$

These approximations are possible due to the simple nature of the basis functions and the fact that the segmentation is uniform across the conducting surface.

3.9 Calculation of the Far Field Radiation Patterns

Electric Field of a Horizontal Electric Dipole

The radiated electric field pattern is calculated by first considering a horizontal electric dipole (HED) oriented in the *u* direction on the surface of the dielectric substrate. We have already seen that the electric field can be expressed as a vector potential and scalar potential by the equation:

$$\vec{E} = -j\omega\vec{A} - \nabla V \tag{3.9.1}$$

to which the usual Lorentz Gauge is imposed

$$\nabla \cdot \vec{A} = -j\omega\mu\varepsilon V \tag{3.9.2}$$

Finally, then, the electric field for a HED on the air-dielectric interface is given by the equation:

$$\vec{E} = -j\omega\vec{A} + \frac{1}{j\omega\mu\varepsilon}\nabla\nabla\vec{A} \tag{3.9.3}$$

The vector potential, $\vec{A}$, created by a HED is given by the Sommerfeld Integral expression of the diadic Green's function, equation.

When the distance between source and observation points is very large, an asymptotic approximation of the Sommerfeld Integral expression of the Green's function can be used. This approximation is obtained using a saddle point method as given in [35]. The final expressions for the electric field has two components. The first component is a spherical wave dominant at angels greater than the grazing angle of $\pi/2$. The other component is a surface wave which travels along the substrate surface. Here, we choose only the first component. Transforming the asymptotic expressions for the Green's function into spherical coordinates, leads to the expressions for the electric field due to a single HED:

$$E_\theta = -\frac{j\omega\mu}{2\pi}\cos\phi\cos\theta\frac{T}{T - j\varepsilon_r\cos\theta\cot k_1 hT}\frac{e^{-jk_1 r}}{r} \tag{3.9.4}$$

$$E_\phi = \frac{j\omega\mu}{2\pi}\sin\phi\cos\theta\frac{1}{\cos\theta - T\cot k_1 hT}\frac{e^{-jk_1 r}}{r} \tag{3.9.5}$$

$$E_r \sim O\left(\frac{1}{r^2}\right) \tag{3.9.6}$$

where

$$T = \left(\varepsilon_r - \sin^2\theta\right)^{\frac{1}{2}} \tag{3.9.7}$$

The mechanism for the radiated field is further approximated to be dominated by the currents on the surface, the effect of currents on the embedded wires are neglected.

Electric Field Due to a Surface Conductor

To simulate the surface conductor with an arbitrary current distribution, an array of the current cells which were used for the method of moments solution of the current distribution is considered. A pattern multiplication approach is the taken to determine the far field due to the conductor. The element patterns are given by the expressions 3.9.4 and 3.9.5. The array factor is then obtained by considering the patch as an array of its composite current cells. Each u directed current cell of the conductor has a current density given by equations (3.2.3) and (3.2.4) which can be written in uv-coordinates as:

$$J_{su} = \frac{1}{\Delta v} \sum_{i=1}^{Nu} I_{ui} T_{ui} \tag{3.9.8}$$

Integrating the roof-top basis function over a current cell gives the result:

$$\frac{1}{\Delta v} \int\int_{S_n} T_{un}(r')\, dS' = \Delta u \tag{3.9.9}$$

The array factor for the current in each direction therefore becomes:

$$\sum_{i=1}^{Nu} \Delta u I_{ui} e^{jk_o(\hat{r} \cdot \hat{r}_i)} \tag{3.9.10}$$

where the values for the current elements, I_{ui}, are obtained directly from the MoM solution

Using the pattern multiplication approach, the normalized far field in each of the E ($\phi = 0$) and H ($\phi = \pi/2$) planes are calculated using the following four equations:

In the E-plane:

$$E_\theta = \frac{T\cos\theta}{T - j\varepsilon_r \cos\theta \cot(k_o hT)} \sum_{i=1}^{Nx} \Delta x I_{xi} e^{jk_o(\hat{r}_i \cdot \hat{x})\sin\theta} \tag{3.9.11}$$

$$E_\phi = \frac{\cos\theta}{\cos\theta - jT\cot(k_o hT)} \sum_{i=1}^{Ny} \Delta y I_{yi} e^{jk_o(\hat{r}_i \cdot \hat{y})\sin\theta} \tag{3.9.12}$$

In the H-plane:

$$E_\theta = \frac{T\cos\theta}{T - j\varepsilon_r \cos\theta \cot(k_o hT)} \sum_{i=1}^{Ny} \Delta y I_{yi} e^{jk_o(\hat{r}_i \cdot \hat{y})\sin\theta} \tag{3.9.13}$$

$$E_\phi = \frac{\cos\theta}{\cos\theta - jT\cot(k_o hT)} \sum_{i=1}^{Nx} \Delta x I_{xi} e^{jk_o(\hat{r}_i \cdot \hat{x})\sin\theta} \tag{3.9.14}$$

4 Modelling Feeds, Loads and Active Devices

4.1 Line Fed Antennas and Devices

A common way to feed an antenna, especially in the environment of an array, is by microstrip line, as shown in figure 4.1.1. Practically, the line is fed via some kind of connector, making a transition from the transmit electronics to the feed line. This is the same mechanism for feeding MIC circuits and devices. A very simple model is used here to represent this type of feed, in which a voltage source is placed in series with the microstrip line. Using the example of a feed line oriented in the x-direction, the source is set to unit magnitude and zero phase and the separation in the line at the source is specified to have zero width. The following expression for the impressed electric field on the segment containing a source in the x-direction is:

$$E^{i}_{xi} = \delta(\hat{r}_{xi}) \qquad (4.1.1)$$

As currents will only exist on the surface of the substrate, the matrix equation 3.7.7 takes on the form:

$$\begin{bmatrix} Z_{xx} & Z_{xy} \\ Z_{yx} & Z_{yy} \end{bmatrix} \begin{bmatrix} I_x \\ I_y \end{bmatrix} = \frac{Z_0}{2\pi} \begin{bmatrix} V_x \\ V_y \end{bmatrix}^T \qquad (4.1.2)$$

When testing with the razor function is imposed on equation 4.1.1, the excitation vector obtained has zeroes at all entries except for a unit element over the excited segment:

$$[V] = [\ldots 0\ 0\ 1\ 0\ 0\ 0 \ldots] \qquad (4.1.3)$$

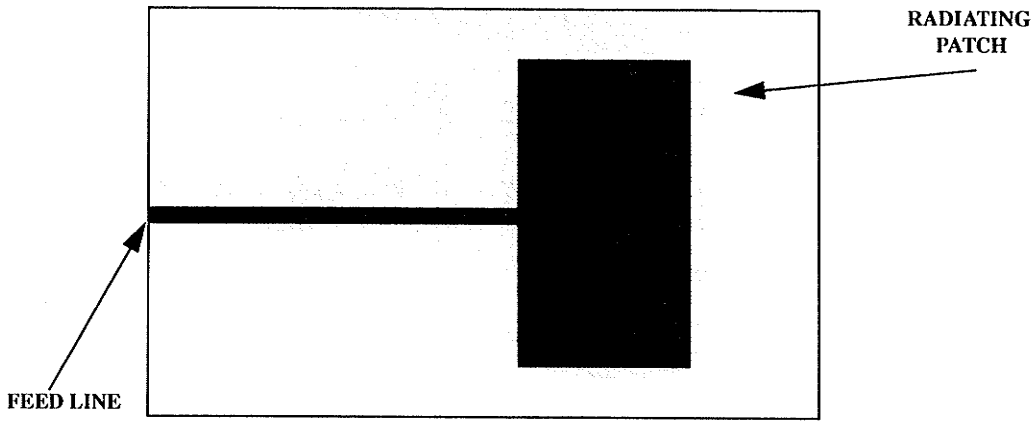

Fig. 4.1.1 Line Fed Microstrip Patch Antenna

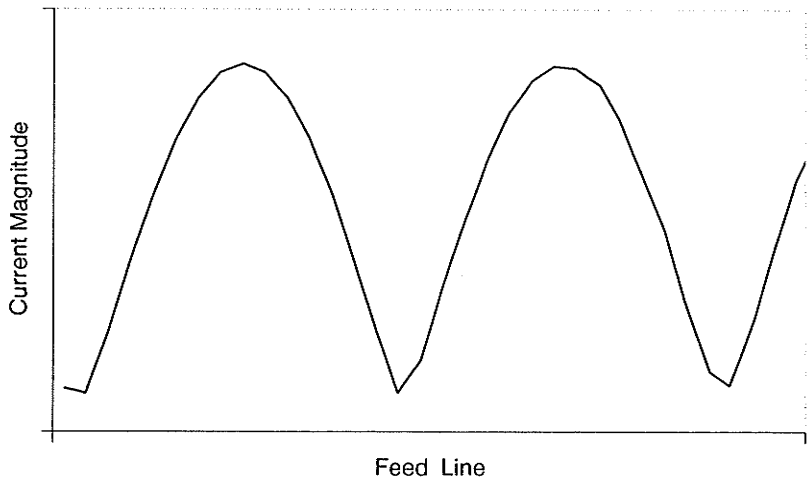

Fig. 4.1.2 Example of a Current Standing Wave on the Microstrip Line

Using this type of excitation the input reflection coefficient of the device is found through studying the current magnitudes on the line.The standing wave ratio (SWR) is obtained by comparing the maximum and minimum value of the current standing wave pattern on the line as shown in figure 4.1.2. The current is approximated as a cubic function local to the points where the maximum and minimum on the line occur. The coefficients of this cubic function are determine by studying the basis function coefficients around these points. The actual locations of the maxima and minima are found using a Newton-Raphson root finding algorithm to find where the derivative of the cubic function is zero. Finally, the input reflection coefficient at a reference point, x_r, is determined by:

$$SWR = \frac{I_{max}}{I_{min}} \tag{4.1.4}$$

$$\left|\Gamma_{in}(x_r)\right| = \frac{SWR - 1}{SWR + 1} \tag{4.1.5}$$

$$\phi(\Gamma_{in}(x_r)) = \beta(x_r - x_{max}) \tag{4.1.6}$$

In the above phase equation, β is obtained by finding the distance between two consecutive current maxima which will be one half of the line wavelength. Then

$$\beta = \frac{2\pi}{\lambda} \tag{4.1.7}$$

One final point to note here is that when the input reflection coefficient is required, the geometry must be such that there are at least two maxima on the line. For the results found in subsequent chapters a feed line of one wavelength at the lowest frequency considered was used.

4.2 Coaxial Feeds

A coaxial pin is also often used for feeding a microstrip patch antenna. Using this method the transmission line and electronics can be kept behind the radiating element and therefore do not interfere with the radiation from the patch. In simulating a coaxial feed, the vertical current elements and a junction as described in the previous chapter are utilized. The coaxial pin extends from the ground plane to the surface conductor as shown in figure 4.2.1. Using the equivalence principle, the outer radius of the coaxial cable can be enclosed by the ground plane and replaced by an equivalent frill of magnetic current [30] as shown in figure 4.2.2

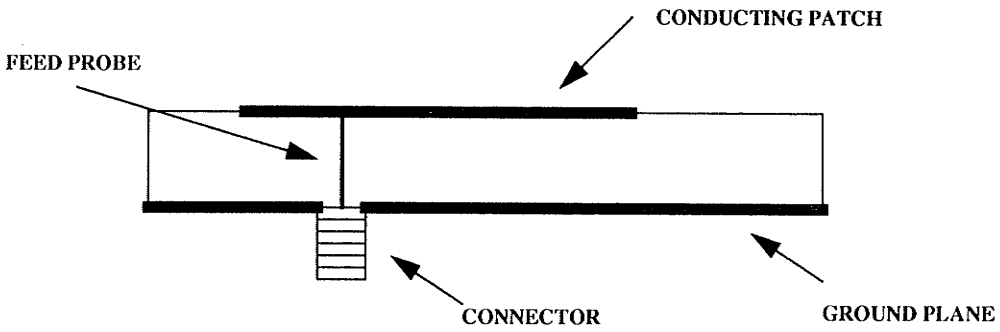

Fig. 4.2.1 Probe Fed Microstrip Patch

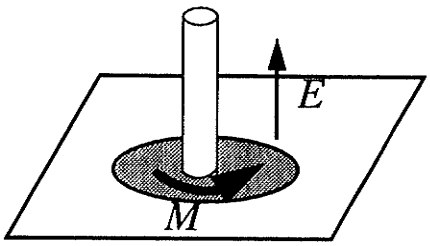

Fig. 4.2.2 Frill of Magnetic Currents in the Ground Plane

Then, the electric field created by this frill of current is analytically calculable. Only the vertical component is considered, which is given by the expressions.

$$M_{\phi} = \frac{-2V}{\rho \ln\left(\frac{b}{a}\right)} \tag{4.2.1}$$

$$E_z(\rho=0, z_o) = \frac{V}{\ln\left(\frac{b}{a}\right)}\left(\frac{e^{-jk_0\sqrt{\varepsilon_r\left((z_0+h)^2+a^2\right)}}}{\sqrt{(z_0+h)^2+a^2}} + \frac{e^{-jk_0\sqrt{\varepsilon_r\left((z_0+h)^2+b^2\right)}}}{\sqrt{(z_0+h)^2+b^2}} \right) \tag{4.2.2}$$

Where a and b are the radius of the coaxial pin and the radius of the opening at the ground plane respectively.

As a result of this form of feed, the excitation vector calculated will be zero for test segments corresponding to the surface conductor at the interface, and for test segments corresponding to the wire and junction.

$$V_i = \int_{z_a}^{z_b} E_z dz \tag{4.2.3}$$

The input impedance is then found simply by Ohm's law dividing the voltage specified on the coaxial line by the current found on the pin, at the ground plane.

$$Z_{in} = \frac{V_{ex}}{I_{in}} \tag{4.2.4}$$

In the case of both the coaxial probe feeding configuration and the passive loading as presented in the next section, the matrix equation takes on the form:

$$\begin{bmatrix} Z_{xx} & Z_{xy} & Z_{xz} & Z_{xj} \\ Z_{yx} & Z_{yy} & Z_{yz} & Z_{yj} \\ Z_{zx} & Z_{zy} & Z_{zz} & Z_{zj} \\ Z_{jx} & Z_{jy} & Z_{zj} & Z_{jj} \end{bmatrix} \begin{bmatrix} I_x \\ I_y \\ I_z \\ I_j \end{bmatrix} = \begin{bmatrix} 0 \\ 0 \\ V_z \\ 0 \end{bmatrix}^T \tag{4.2.5}$$

where the calculation of V_z is performed as above. The full expressions for the various components of this matrix are also give in Appendix A.

4.3 Passive Loading

Often, a microstrip circuit contains discrete elements on the surface used for matching devices. Pins and other reactive loads between the conducting patch and the ground plane have be recently used to increase the bandwidth of microstrip antennas as well. A simple model may be constructed of a passive load at any point where the current is continuous in one direction as in figure 4.3.1 below.

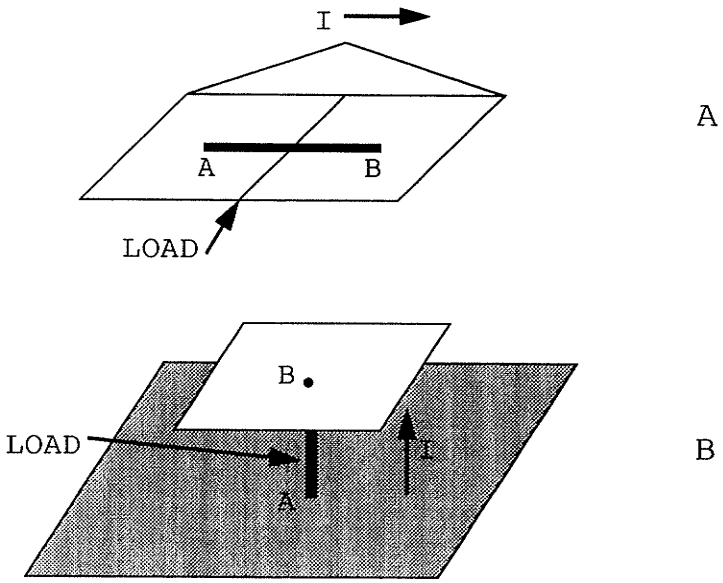

Fig. 4.3.1 Loads Parallel (A) and Perpindicular (B) to the Conducitng Surface

The effect of the load is a change of electric field where the load is placed. This field takes the form of [31]:

$$E = \frac{-V_L}{\Delta l} \qquad (4.3.1)$$

Where V_L is the voltage drop across the load which is described by Ohm's law $V_L = Z_L I_L$ and Δl is the linear distance over the conductor where the load exists.

The current in the loaded cell is a function of currents in adjacent cells and thus the expression for the field at a loaded cell should reflect this. This results in a complicated expression of the field including different elements. However, if the load is considered to be concentrated in the infinitesimal gap between the charge cells of the loaded current cell, the mathematical description of the load can be simplified so that it only affects one term of the moments matrix [32]. In this case then,

$$\grave{\mathbf{E}} = -V_L \delta(\grave{r}_L) \tag{4.3.2}$$

This can be added to the impressed field due to all other sources since the media are all linear. The right hand side of the MPIE is then altered to reflect this and the testing function is applied.

$$\int_{C_i} \grave{\mathbf{E}} \cdot dl = -V_L + \int_{C_i} \grave{\mathbf{E}}_s \cdot dl = -Z_L I_i + \int_{C_i} \grave{\mathbf{E}}_s \cdot dl \tag{4.3.3}$$

Where C_i is segment that is loaded and $\grave{\mathbf{E}}_s$ is the field due all sources. The term containing the impedance and current is placed in the matrix. Since the impedance only acts on the current directly corresponding to the test segment where the load is placed the terms in the moments matrix except the self term corresponding to the loaded current cell remain the same and that self term becomes, for loads on the surface in the x-direction

$$Z_{xx}(i,i) = Z_{xx}(i,i) + Z_L . \tag{4.3.4}$$

When the load exists between the conducting surface and the ground plane, within the dielectric subtrate, two cases may be considered. If the load is a given value, as for the case of a diode or inductor for example. A current may placed on the surface of the conductor using the function describing the wire-patch junction, with magnitude I_j. The voltage drop at the load point can then be expressed in two ways. First using Ohms law:

$$V = Z_L I_j \tag{4.3.5}$$

Then, by expressing the voltage as a function of the z-directed electric field,

$$V = \int_{-h}^{0} E \cdot dl \tag{4.3.6}$$

Finally the electric field is expressed in terms of its vector and scalar potentials

4.4 Simplification of Coaxial Feeds and Loads

Considerable savings of both time and memory can be obtained by using a simple approximation of the current on the wire part of a coaxial feed or load. By considering that when is the substrate layer is thin ($< \lambda/10$), and hence the wire section is short, the current on the wire can be considered to be constant. Assuming this allows the wire current and the

junction current to be represented by a single value. In turn, this eliminates the need to calculate the effect of wire sections on other wire sections as well as effects of surface cells on the wire sections and vice versa. With this approximation the matrix equation becomes:

$$\begin{bmatrix} Z_{xx} & Z_{xy} & Z_{xj} \\ Z_{yx} & Z_{yy} & Z_{yj} \\ Z_{zx} & Z_{zy} & Z_{zj} \end{bmatrix} \begin{bmatrix} I_x \\ I_y \\ I_z \end{bmatrix} = \begin{bmatrix} 0 & 0 & V_z \end{bmatrix} \qquad (4.4.1)$$

Where the components of the Z matrix are given in Appendix A keepeing in mind that a test segment along wire components now extends from the conductor to the ground plane. It should also be noted here that as the thickness of the substrate increases the approximation will become less and less valid.

4.5 Integration of Active Devices

Active devices have been successfully integrated into the characterization of microstrip structures using time domain methods [33]. In these methods, the two device ports are usually modelled by a load on one port and a voltage dependent current source on the other. Then the time domain fields on the affected segments are formulated using differential equations. The models used in these methods are usually extracted using the small signal parameters of the device (S-parameters or Y-parameters). In extracting this model, it is sometimes possible to add elements which are not necessarily part of the device or, conversely, to omit part of the device due to over simplification. In the frequency domain, the Z-parameters may been used to describe the two port device without the formation of an equivalent circuit model. A frequency domain model for an active device

has been given [34] where a pin is connected to the ground plane and becomes a common point for the two ports of the device. Again this pin may add something erroneous to the device that is being described. Instead of adding this complication, the device may be thought of as a "black box" where the parameters given are external responses to external conditions. Using this model, the device may be thought of as simply a two port as shown in figure 4.5.1

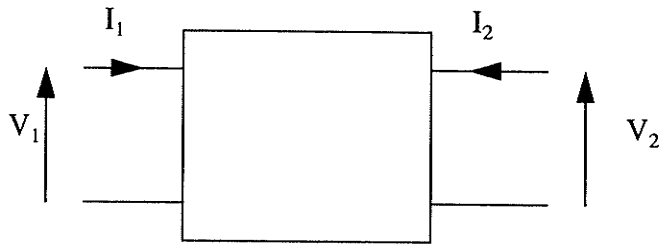

Fig. 4.5.1 General Two Port Device

The port voltages and currents are linked through the network Z-matrix by

$$\begin{bmatrix} V_1 \\ V_2 \end{bmatrix} = \begin{bmatrix} Z_{11} & Z_{12} \\ Z_{21} & Z_{22} \end{bmatrix} \begin{bmatrix} I_1 \\ I_2 \end{bmatrix} \qquad (4.5.1)$$

Then, by adding current to the points where the device is connected, the external response is given. These currents are added in the form of the junction current basis functions on the surface conductor introduced in an earlier chapter. Finally, the port

voltages are determined by integrating the z-directed electric field determined by all the surfaces currents and charges from the point of device contact to the ground plane.

$$V = \int \mathbf{E} \cdot dl \tag{4.5.2}$$

For each of the two ports, then, an equation can be defined that looks somewhat like the MPIE, that is

$$\int_{-h}^{0} \left(-j\omega A_z - \frac{dV}{dz} \right) \Big|_{port(i)} dl = Z_{ii} I_i + Z_{ij} I_j \tag{4.5.3}$$

Using the same linearization method described in the previous chapter, the system of equations is increased by two extra equations for each device present. Some additions also are needed in the existing system of equations. The main goal in this formulation is to ensure the continuity of the surface current of the device and the surface conductor. The matrix components corresponding to wire-device and junction-device interations are assumed negligible The final linear system will then have the form

$$\begin{bmatrix} Z_{xx} & Z_{xy} & Z_{xz} & Z_{xj} & Z_{xd} \\ Z_{yx} & Z_{yy} & Z_{yz} & Z_{yj} & Z_{yd} \\ Z_{zx} & Z_{zy} & Z_{zz} & Z_{zj} & 0 \\ Z_{jx} & Z_{jy} & Z_{jz} & Z_{jj} & 0 \\ Z_{dx} & Z_{dy} & 0 & 0 & Z_{dd} \end{bmatrix} \begin{bmatrix} I_x \\ I_y \\ I_z \\ I_j \\ I_d \end{bmatrix} = \begin{bmatrix} V_x \\ V_y \\ V_z \\ V_j \\ 0 \end{bmatrix} \tag{4.5.4}$$

- The additional elements in the moments matrix are given in Appendix A

5 Numerical Results

5.1 Introduction

In this chapter some known measured results as well as analytic and approximate solutions are used to test the accuracy and flexibility of the methods developed and used for the generation of the microstrip analysis tool as described in the preceding chapters. The first section deals with some preliminary investigations that have been performed in order to verify that the solutions produced are consistent with analytic solutions and approximations such as transmission line theory. This section covers models for the line fed and coaxial cable fed structures as well as the passive and active loading as has been given in chapter 4. A simple check against an analytic solution is also performed to verify the calculation of the far field patterns as developed in chapter 3. The remainder of the chapter is used to compare results for specific designs that have been tested by various other researchers. Study of new antenna design is beyond the scope of the project, any design used is solely to test the accuracy and versatility of the model.

5.2 Validation of the Model

Current Distributions

In order to confirm that results produced are in accordance with what is theoretically expected, a preliminary study is undertaken, using the method to analyse the currents on a thin wire dipole over a ground plane. It is well known that for this configurations current magnitude at the end points on the dipole will be minimum, but not quite zero due to fringing effects. The additional minima on the line will occur at points one half of the line wavelength apart, similarly for the maxima. With this in mind, the method was used to analyse a centre fed, thin wire dipole of length 2λ and width $\lambda/100$, over a ground plane at height $(\lambda/100)$ as shown in figure 5.2.1.

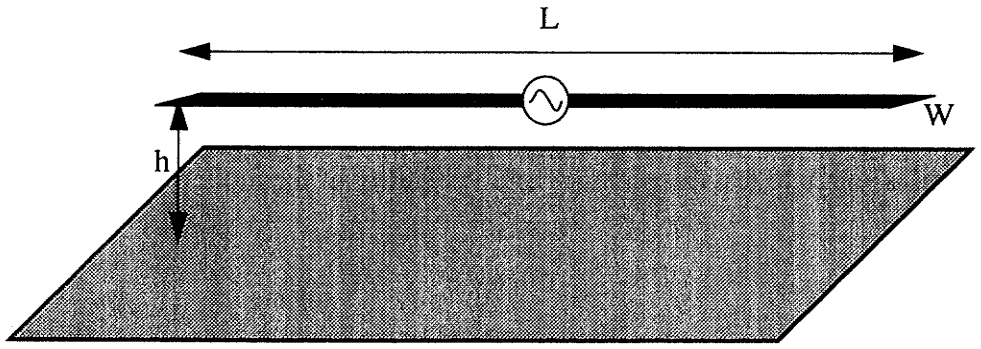

Fig. 5.2.1 Centre Fed Dipole Over Ground Plane

To check the convergence of the results, the analysis was performed using 10, 20, 40 and finally 100 segments/λ. Figure 5.2.2 shows that the values for the magnitude and locations of maxima and minima are consistent with theoretical expectations over all four segmentation schemes. The figure also demonstrates that the method is convergent for increasingly accurate models, in fact the curves for 40 and 100 segments per wavelength are almost indistinguishable.

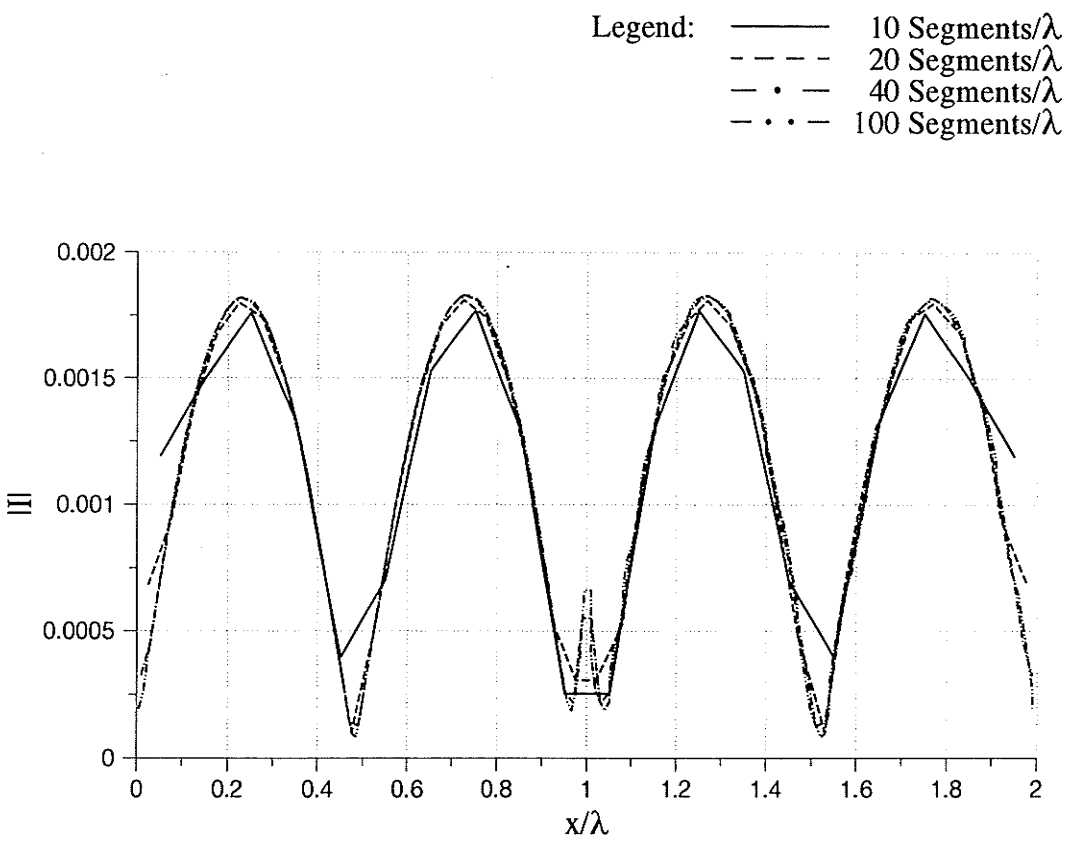

Fig. 5.2.2 Currents on the Centre Fed Dipole

Input Reflection Parameters

A second test is performed to verify the method of obtaining the input S-parameter of a microstrip structure fed by microstrip line. For an open circuited line, the magnitude of the S_{11} parameter will be unity while the angle of the S_{11} parameter will be dependent on the frequency of excitation and the plane of reference that the reflection parameter is measured at, according to the equation:

$$angle\,(S_{11}) = \left[\frac{4\,(x_{oc} - x_{ref})}{\lambda}\right] 180 + 180 \qquad (5.2.1)$$

Furthermore, if a load such as a two parallel open circuited stubs is placed at the end of the line, the S_{11} parameter seen by the feed line can be calculated from.

$$S_{11} = \frac{Z_L - Z_o}{Z_L + Z_o} \qquad (5.2.2)$$

where Z_0 is the characteristic impedance of the microstrip line and Z_L is calculated using the impedance transformation equation:

$$Z_L = \frac{Z_T + jZ_o \tan\beta l}{Z_o + jZ_T \tan\beta l} \qquad (5.2.3)$$

and the load of the parallel open circuited lines, Z_T, is calculated from:

$$Z_T = \frac{1}{2} jZ_o \cot\left(\frac{2\pi l}{\lambda}\right) \qquad (5.2.4)$$

With this in mind, two simulations are performed, in the first, a one wavelength line was fed at one end over a 20% bandwidth of the centre frequency the height of the substrate is $\lambda/100$. The result for the S_{11} parameter of the open circuit line using fifty (50) segments per wavelength along with the analytical result is given in figure 5.2.3. In the second test, a one wavelength feed line connected to the centre of a perpendicular line of one half the wavelength at the centre frequency is examined over a 20% bandwidth of the centre frequency using the same height and segmentation scheme. In both cases, the The S_{11} parameters of the calculated and analytic results for this simulation are also given in figure 5.2.3. While the cubic spline approximation of the current distribution on the feed line proves to be somewhat inaccurate, giving a non-unity magnitude for S_{11}, an agreement to within 5% is obtained and results for the phase of the S_{11} parameter are accurate to within 5 degrees.

Also of note in this comparison is the fact that the transmission line model cannot account for fringing effects at the open circuit end. In fact if the line length were increased, the phase of the S_{11} parameter would be more in line with what was calculated using the present method. For the phase of the scattering parameter, the presented method provides more accuracy than the transmission line model.

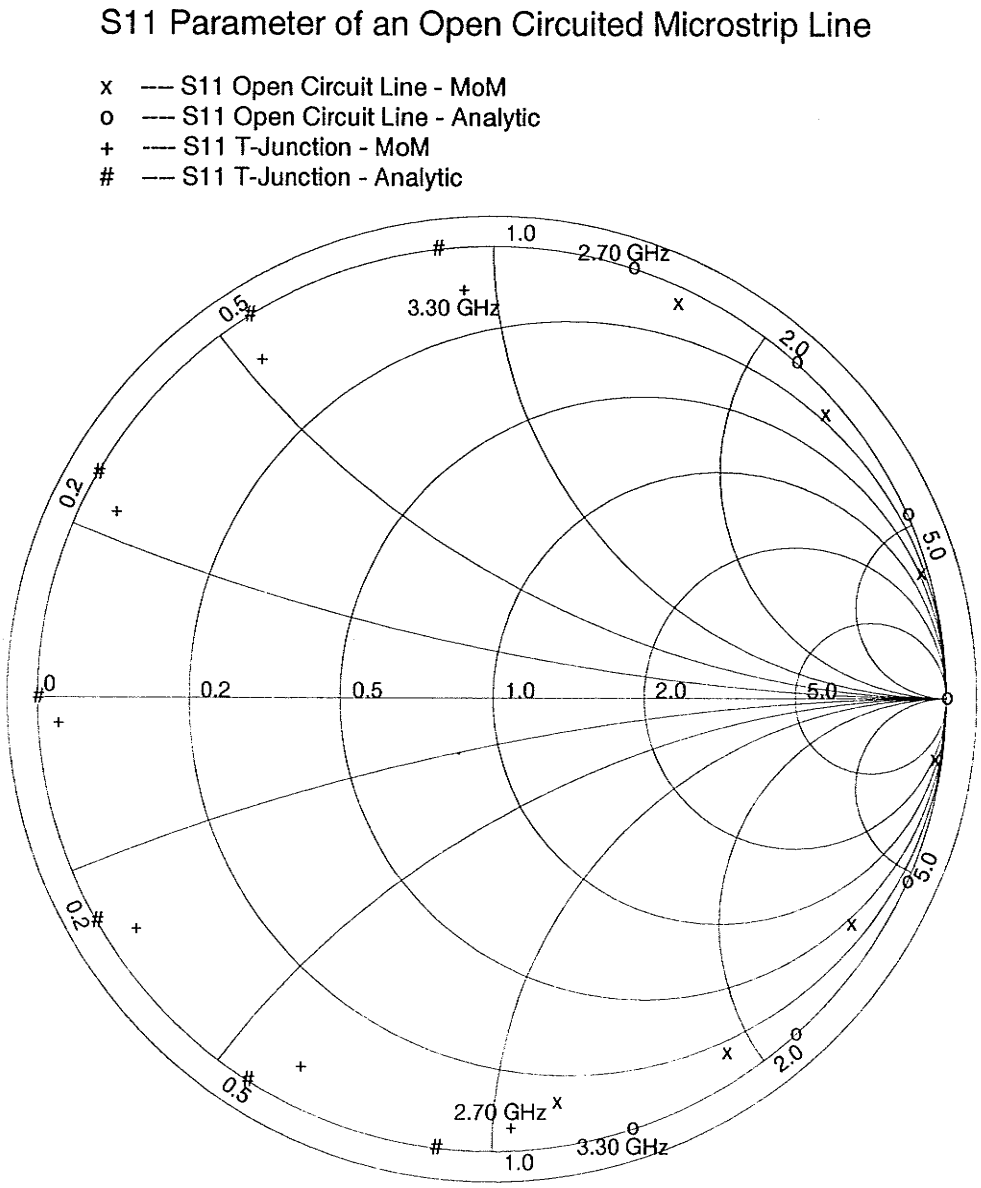

Fig. 5.2.3 S11 Parameters for an Open Circuit and Microstrip Circuits

Input Impedance Coaxial Pin Fed Microstrip Structures with Loads

The third test is performed to verify the result for the input impedance of the coaxial pin fed microstrip structures as well as for loads placed on the microstrip structure. The impedance of a microstrip line that is either open circuited, short circuited or loaded with a known impedance can be found easily using transmission line theory. A well known low frequency approximation for the input impedance Z_{in} of a loaded transmission line with characteristic impedance Z_0, can be obtained from the equation [42]:

$$Z_{in} = Z_0\left[\frac{Z_L + jZ_0\tan(\beta x)}{Z_0 + jZ_L\tan(\beta x)}\right] \tag{5.2.5}$$

Where Z_L is the impedance of the load placed on the line, β is the propagation constant of the transmission line, $2\pi/\lambda_d$, and x is the length of the transmission line between the source and the load. This provides a good analytic result with which to compare values obtained using the method and models developed.

With this in mind, a microstrip line was modelled, the line is designed to have a characteristic impedance of 50 Ohms. The dielectric substrate is lossless with $\varepsilon_r = 2.59$ and a height of 1.59 mm. The line is one wavelength at 1Ghz and is fed by coaxial pin at one end as shown in figure 5.2.4.

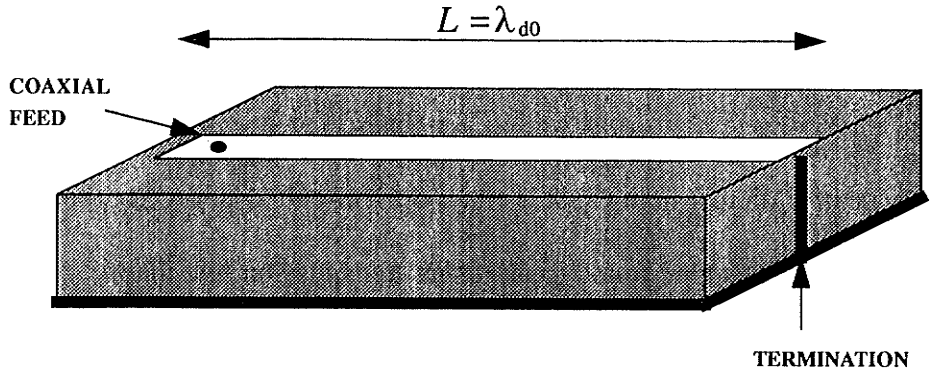

Fig. 5.2.4 Microstrip Line Used for the Verification of Loaded Result

The results for the input impedance over a 20% bandwidth about the centre frequency for the open circuited and short circuited lines using fifty segments per wavelength are given on the Smith chart of figure 5.2.5. The Smith chart plot of figure 5.2.6 displays results for a matched load and for an arbitrarily chosen termination of a resistance of 10 Ohms in series with an inductance of which would add to the impedance an imaginary part of j10 Ohms at the centre frequency. These results are compared to the transmission line theory results and demonstrate the an agreement between theory and the method to within about 2.5% of the frequency in the worst case. Once again, because of the neglect of the fringing field in the transmission line model, the phase of the impedance as calculated by the present method will be more reliable than that calculated using the transmission line model.

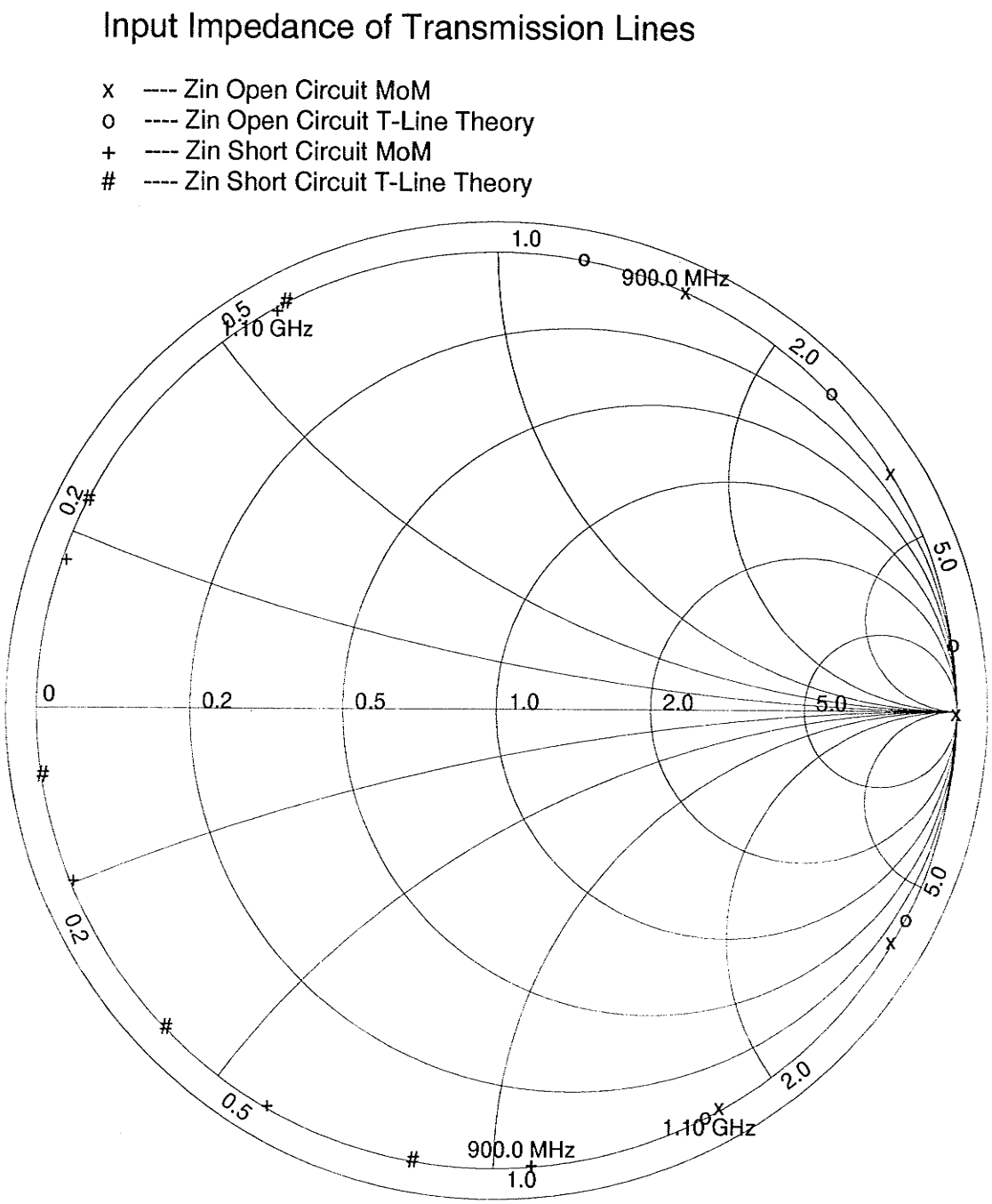

Fig. 5.2.5 Transmission Line Theory and Moment Method Results for the Input Impedances of Open Circuited and Short Circuited Microstrip Lines

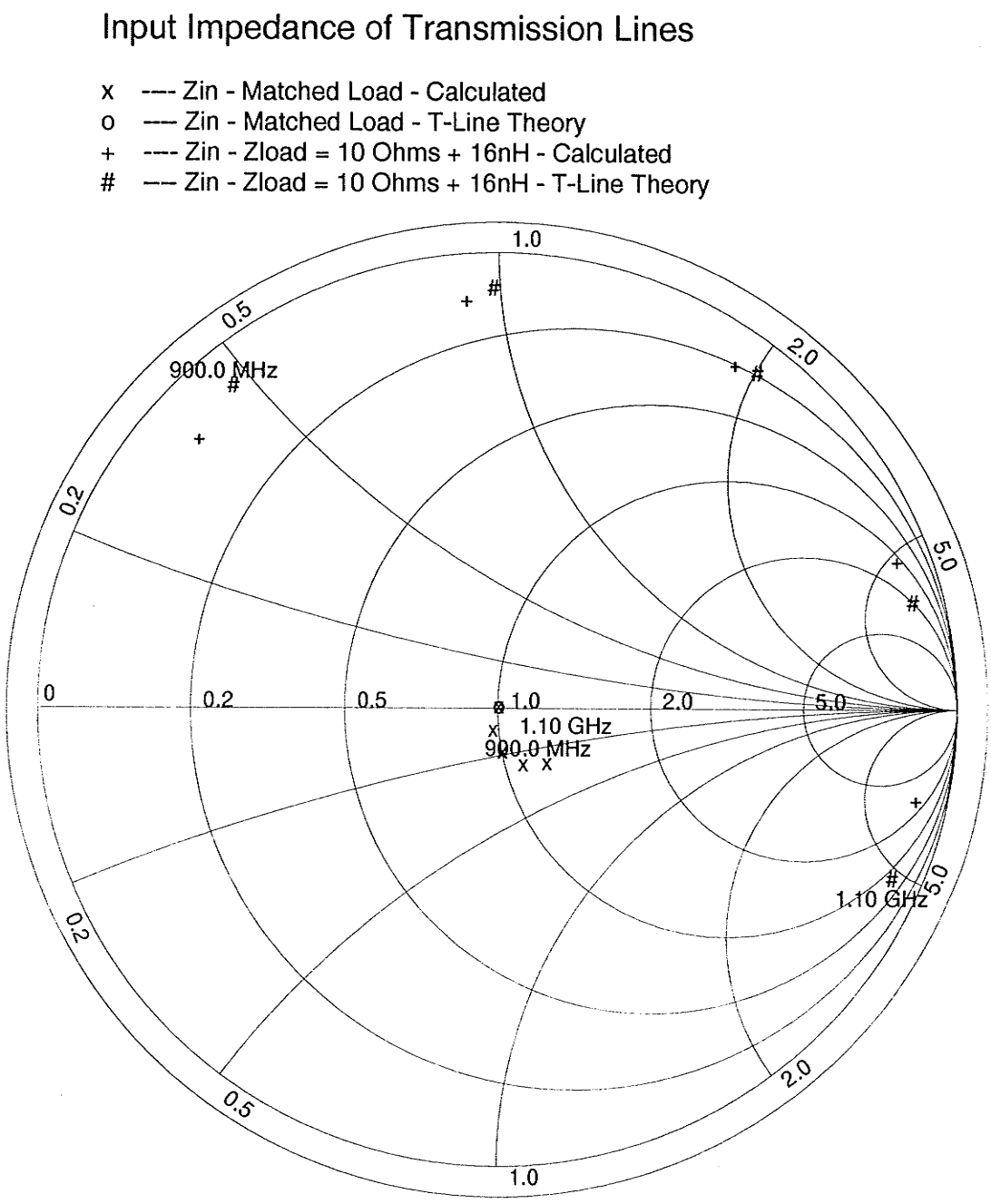

Fig. 5.2.6 Transmission Line Theory and Moment Method Results for the Input Impedances of a Microstrip Line with Two Different Load Schemes

Radiation Patterns

A final test is performed to verify the result for the radiation pattern as obtained using the methods described in chapter 5. For this test, the analytic result for a half-wave dipole over a ground plane is used to compare to the calculated result. A well known analytic approximation for the radiation pattern of a thin wire dipole a antenna is given by the following formula [41]:

$$H_\phi(\theta) = \frac{E_\theta(\theta)}{\eta} \propto \frac{\cos\left(\frac{kl}{2}\cos\theta\right) - \cos\left(\frac{kl}{2}\right)}{\sin\theta} \tag{5.2.6}$$

where θ is the elevation angle, k is the wave number, $2\pi/\lambda$ an l is the length of the dipole. This result is multiplied by an array factor to account for the effect of the ground plane. The array factor is obtained by considering an isotropic source and its image on the other side of the ground plane separated by a phase of 180 degrees and a distance of twice the substrate height. This array factor will therefore have the form.

$$AF(\theta) \propto \cos\left(\frac{1}{2}(k(2h)\cos\theta - \pi)\right) \tag{5.2.7}$$

Where h is the substrate height. The H-plane pattern is determined analytically by considering only the array factor

The method is used calculate the patterns of a thin microstrip dipole 100 mm long and 0.5 mm wide, 5 mm above a ground plane.Simulations are performed for the microstrip dipole operating as a half-wave dipole (1.5 Ghz) and as a one and one quarter wave dipole (3.75 GHz). Results obtained using the method described in chapter 5 are compared to the analytic result obtained using equations 5.2.6 and 5.2.7. Figures 5.2.7 and 5.2.8 show an excellent qualitative agreement in both planes of the radiation patterns, with the Moments Method result indistinguishable from the analytic result in all cases but for the dipole operating at 3.75 GHz. This result was included to demonstrate the amount of discrepancy for a pattern with nulls. An error of about 2 degrees is observed in the position of the nulls and the magnitudes of the second lobes differ by about 2dB in the range of -15dB, exhibiting still an excellent agreement.

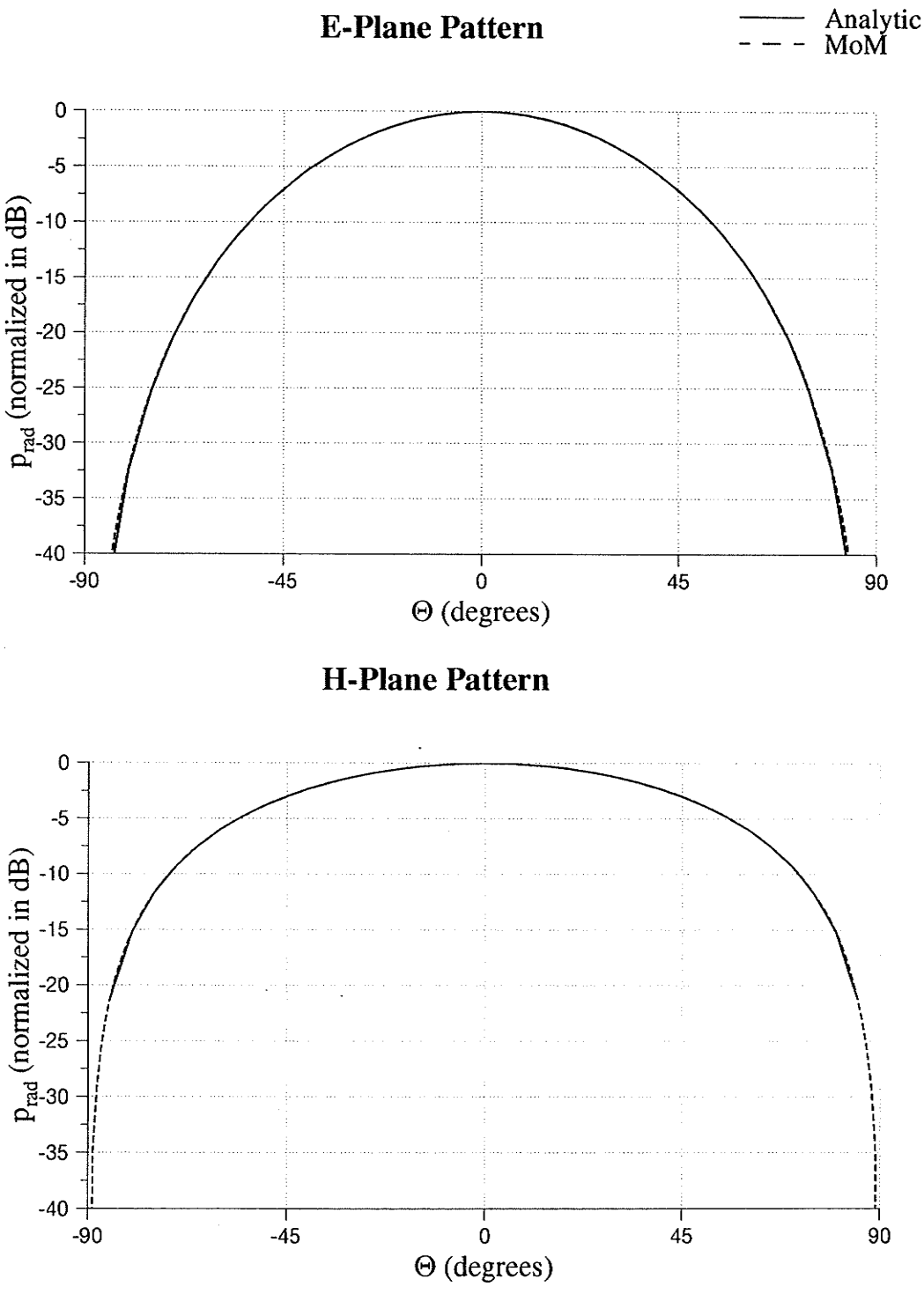

Fig. 5.2.7 Far Field Patterns of a Half-Wave Dipole Over Ground Plane

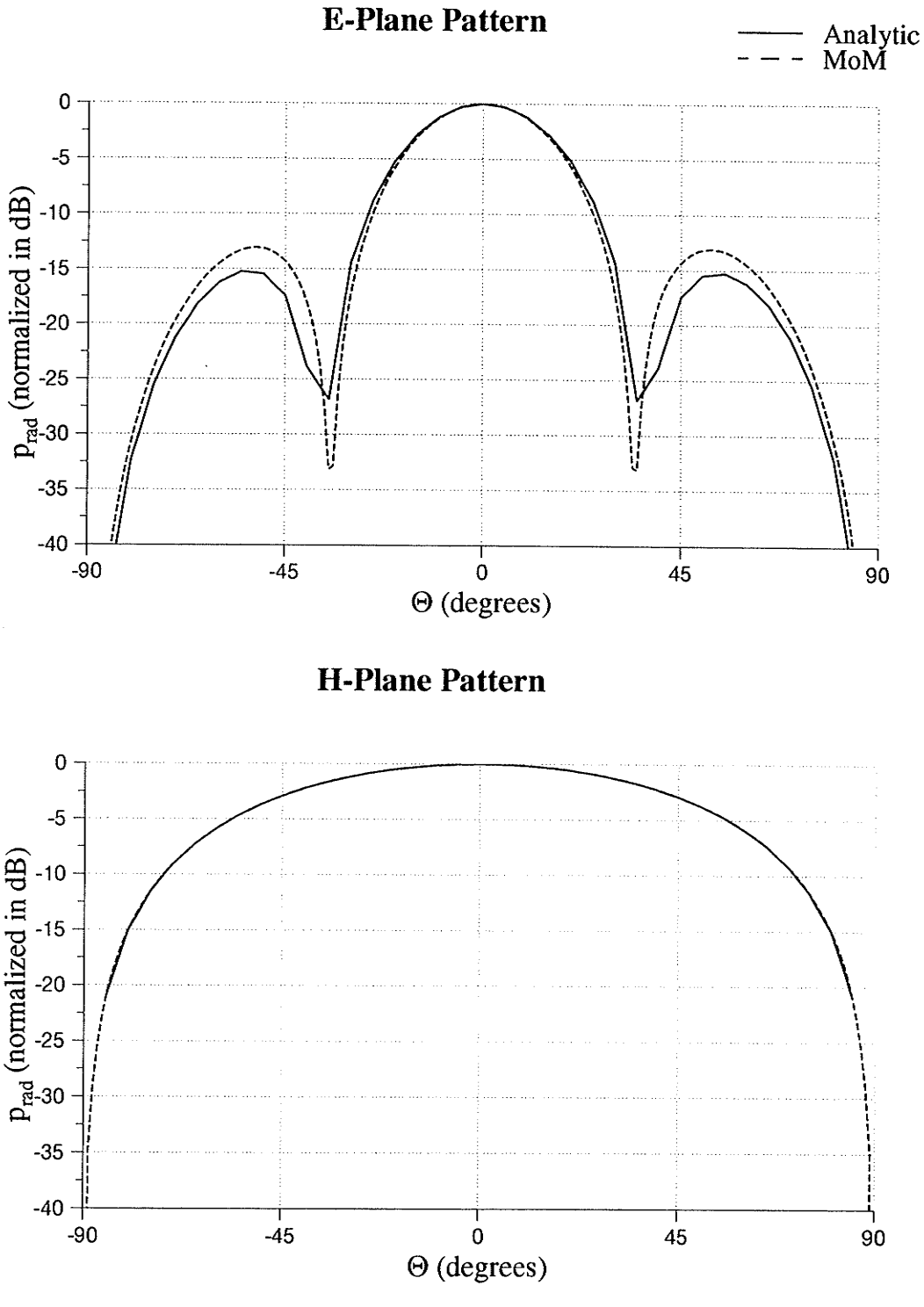

Fig. 5.2.8 Far Field Patterns of a 1.25 λ Dipole Over Ground Plane

5.3 Active Circuits

It is becoming increasingly popular to attempt to create an "active antenna" by combining active elements with resonant microstrip structures. Using this method, the power radiated by the antenna may be increased, and arrays of these elements may create a powerful directive pattern for use in such applications as radar. It may also become important to circuit designers to include their active elements in the full wave model of the circuit as opposed to, for example, creating circuit models of the microstrip line sections and using a circuit simulator to analyse the entire system.

The model of an active load as described in Chapter 4 is one proposal for a method in which such a device may be included in the full wave analysis. Results obtained using the method developed are compared with the input impedance as found by the LADDER program, a program developed in the Electrical Engineering Department at the University of Manitoba which uses a transmission line model. This result is used only to demonstrate that the method developed in chapter 4 provides a reasonably accurate result when compared to well accepted methods.

Figure 5.3.1 shows a transistor connected to a microstrip feed line with a line and 50 Ohm load attached at the output, the transistor reflection coefficients are given in table 5.3.1. The height of the substrate is 1.59 mm and the relative dielectric constant, ε_r, is 2.56. Two cases are studied here, the case of the feed and load lines only attached to the transistor, then the case where tuning stubs are included at input and output to attempt a more close match. The results for the input impedances using a segmentation scheme of twenty segments per wavelength are also given in figure 5.3.1. They demonstrate that the method provides a reasonable agreement with accepted theory, the transmission line model.

Table 5.3.1: Input Parameters for the Transistor Used

f (Mhz)	S11 (mag.)	S11 (ang.)	S21 (mag.)	S21 (ang.)	S12 (mag)	S12 (ang.)	S22 (mag.)	S22 (ang.)
1000	0.60	-154	13.0	87	0.056	35	0.60	-33
1100	0.60	-159	12.3	83	0.057	35	0.59	-34
1200	0.60	-165	11.6	80	0.058	36	0.58	-35
1300	0.60	-169	10.9	76	0.057	36	0.58	-36
1400	0.60	-174	10.3	73	0.058	37	0.57	-37
1500	0.60	-178	9.8	70	0.058	38	0.57	-38

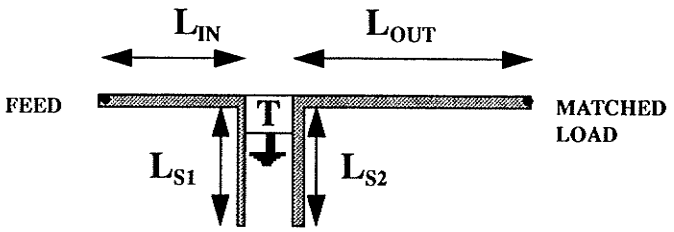

L_{IN} = 15.64 mm
L_{OUT} = 60.34 mm
L_{S1} = 22.35 mm
L_{S2} = 22.35 mm
Z_0 = 50Ω

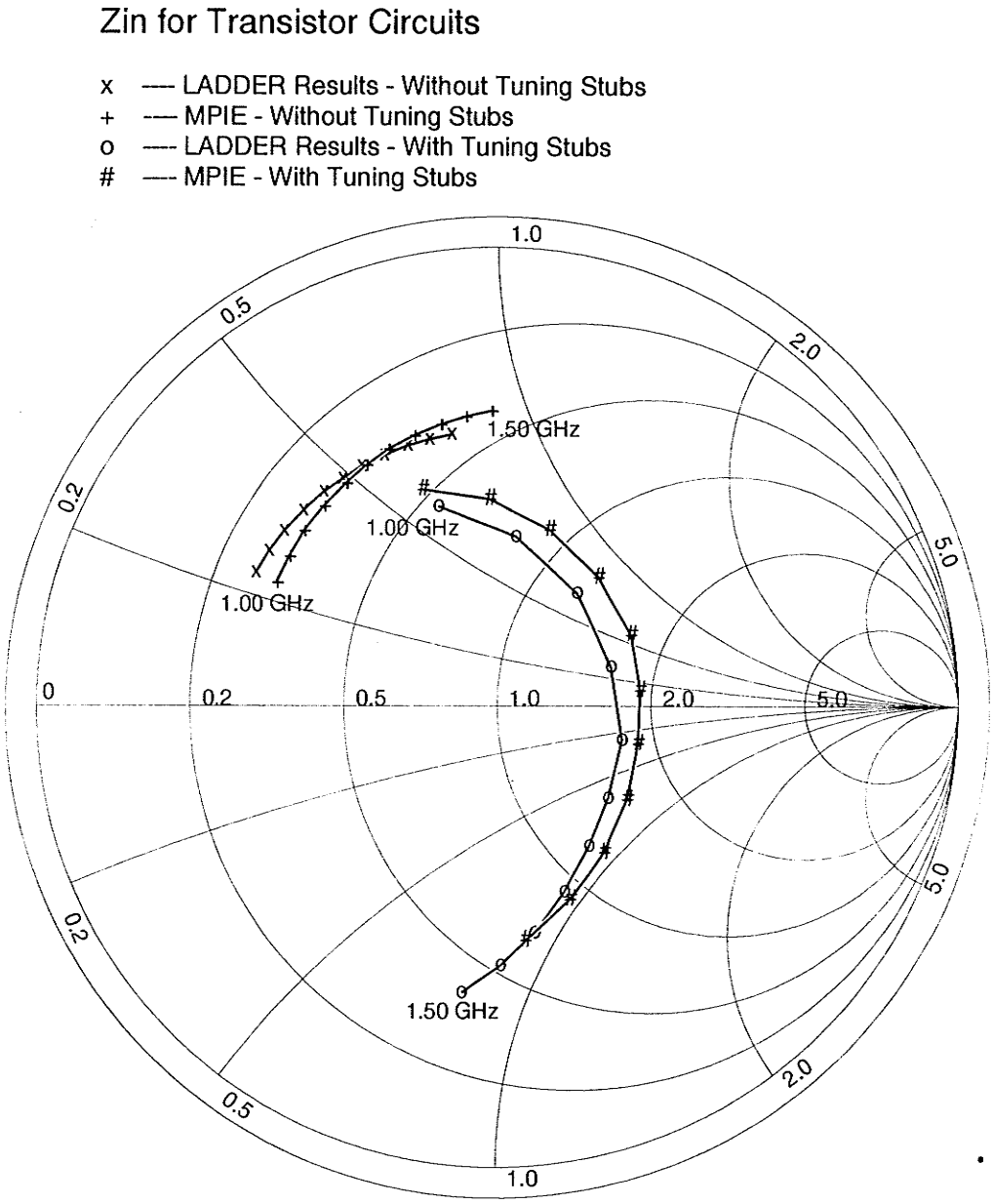

Fig. 5.3.1 Input Impedance for Two Different Active Circuits

5.4 Line Fed Microstrip Patch Antenna

The line feeding configuration consists of simply attaching the patch antenna to a microstrip line. In such a system, the line may be connected at the other end directly to the transmit or receive circuitry or, more commonly, in an array environment with other antennas and lines on the same surface. This method has been studied both numerically and experimentally by several authors [37],[36],[38] and there exists a great deal of both calculated and numerical data for this type of structure.

To obtain a better match between line and resonator, it is common to create an inset feed by removing notches around the contact point between the line and patch. By varying the dimensions of these notches a good match may be obtained. In the past this was done by using some empirical formulae and by prototype testing. Using a software tool such as the one developed, a model may be obtained and the notch dimensions varied on computer rather than successive test runs. Figure 5.4.1 shows a line fed microstrip antenna into which notches may be cut in order to obtain a more desirable match. The method is first used on the feed structure without notches to verify the accuracy of the result, then it is used on the notched structure to demonstrate the flexibility of the method. In each case the patch is segmented using 12x7 segments, meaning that only one cell is missing in the notched case. The results are compared with measured results obtained by Legay [37], shown in figure 5.4.1. Results obtained for the unnotched model show that a close approximation of this structure is possible. However, a large shift in the result for the notched model suggests that a increased segmentation may be needed around the notch area. A method of accomplishing this is prescribed in the next chapter.

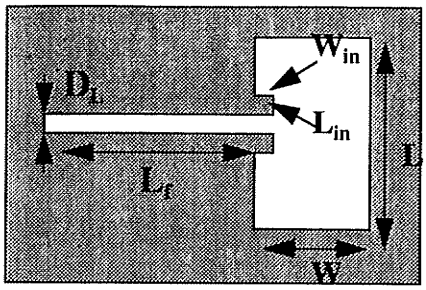

$L = 15.30$ mm
$W = 11.00$ mm
$L_f = 17.86$ mm
$D_L = 2.20$ mm
$h = 0.80$ mm
$\varepsilon_r = 2.17$
$W_{in} = 2.20$ mm
$L_{in} = 1.85$mm

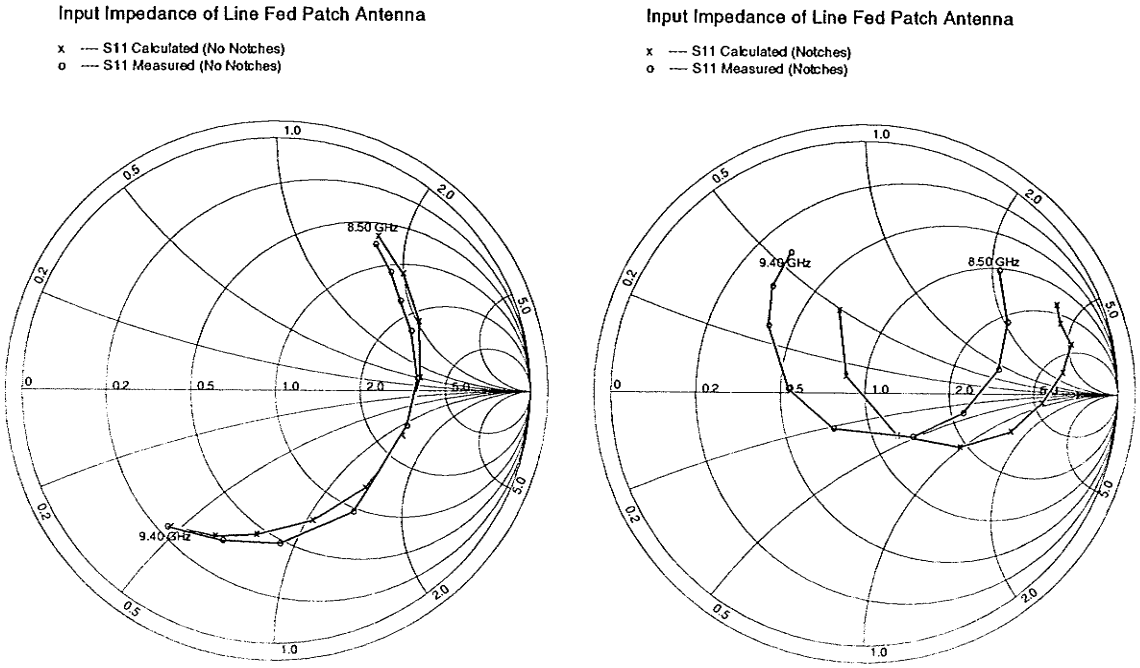

Fig. 5.4.1 S11 for Rectangular Patch Antenna with Inset Line Feed

5.5 Coax Fed Microstrip Patch

When the microstrip patch antenna is fed by coaxial line, there are several effects that contribute to the input impedance. Certainly, it is obvious that the patch dimensions as well as the frequency and the substrate dielectric constant have a great effect. However, several more subtle parameters such as the location of the placement of the probe on the patch and the height of the substrate will also exert themselves. There is, additionally no real analytic method for calculating these impedances and no intuitive result as with some of the previous models calculated. There is, fortunately, a great deal of data both calculated and measured available in the literature dealing with various shapes and sizes of microstrip antennas fed by coaxial probes. One particular paper by Abboud et al. [39] uses cavity models to calculate the input impedance for a range of frequencies and substrate thicknesses. Their calculations are then, in turn, compared with measurements made with fabricated antennas. The comparison with these results, shown in figure 5.5.1, is a low frequency antenna operating at about 660 MHz. The second, shown in figure 5.5.2, is an antenna designed to operate at higher frequencies, about 4.35 GHz. Finally the method is used to analyse a circular antenna in order to test the validity of the method on non rectangular structures, and compared with some measurements performed by Chew et al. [6]. Figures 5.5.1 and 5.5.2 demonstrate that once again the method is accurate to within about 2.5% with respect to frequency for rectangular models. Figure 5.5.3 shows that some accuracy is lost when analysing an irregular structure but that it improves with increased discretization of the conducting surface. All three figures also demonstrate that the method converges toward measured results when the segmentation is increased.

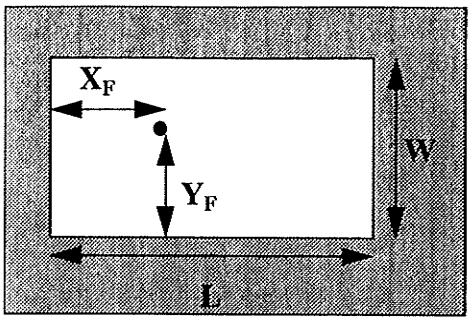

L = 139.7 mm
W = 204.5 mm
X_F = 6.35 mm
Y_F = 102.25 mm
h = 1.588 mm
ε_r = 2.59
$\tan\delta$ = 0.003

Input Impedance of Patch Antenna (139.7mm X 204.5mm)

x —— Zin Calculated - MoM
o —— Zin Measured

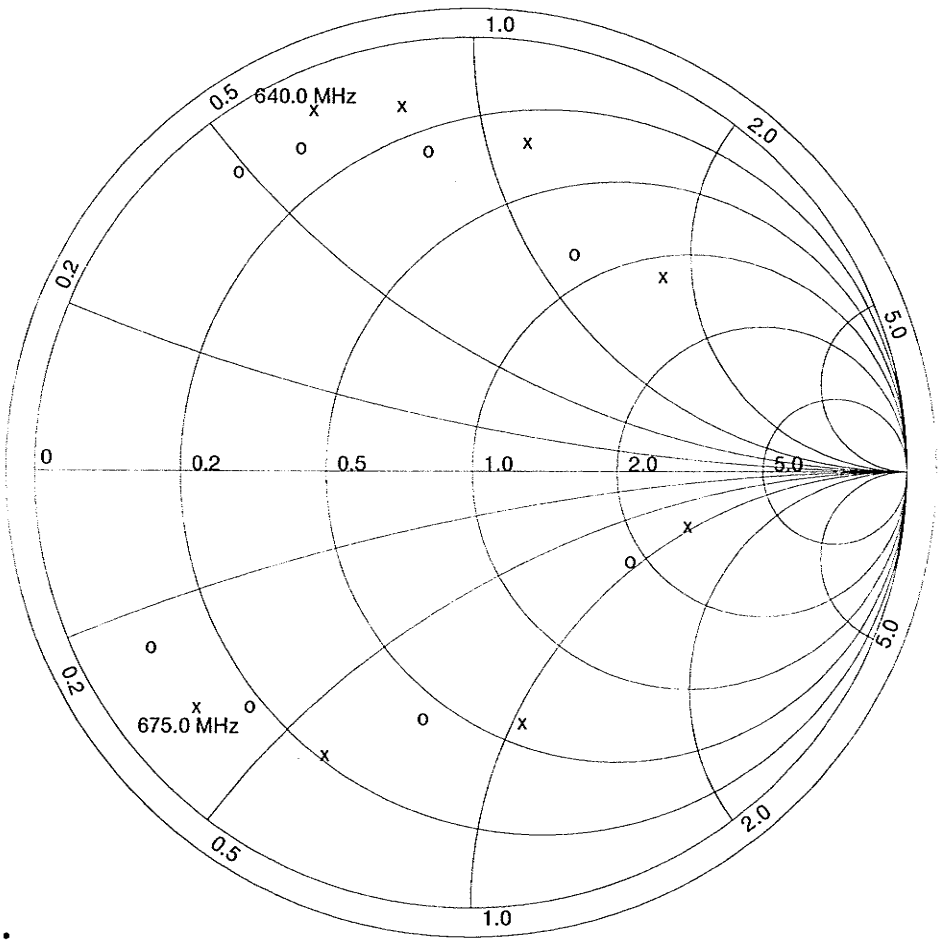

Fig. 5.5.1 Input Impedance for Coax Fed Patch Antenna Resonant at 660 MHz

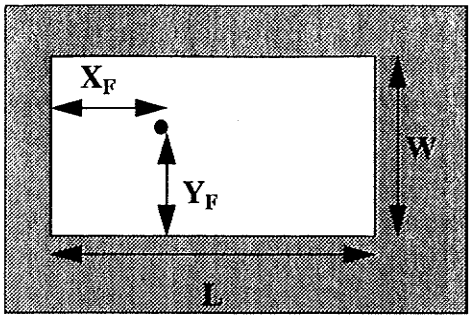

L = 20.1 mm
W = 20.1 mm
X_F = 1.3 mm
Y_F = 10.05 mm
h = 1.59 mm
ε_r = 2.55
$\tan\delta$ = 0.002

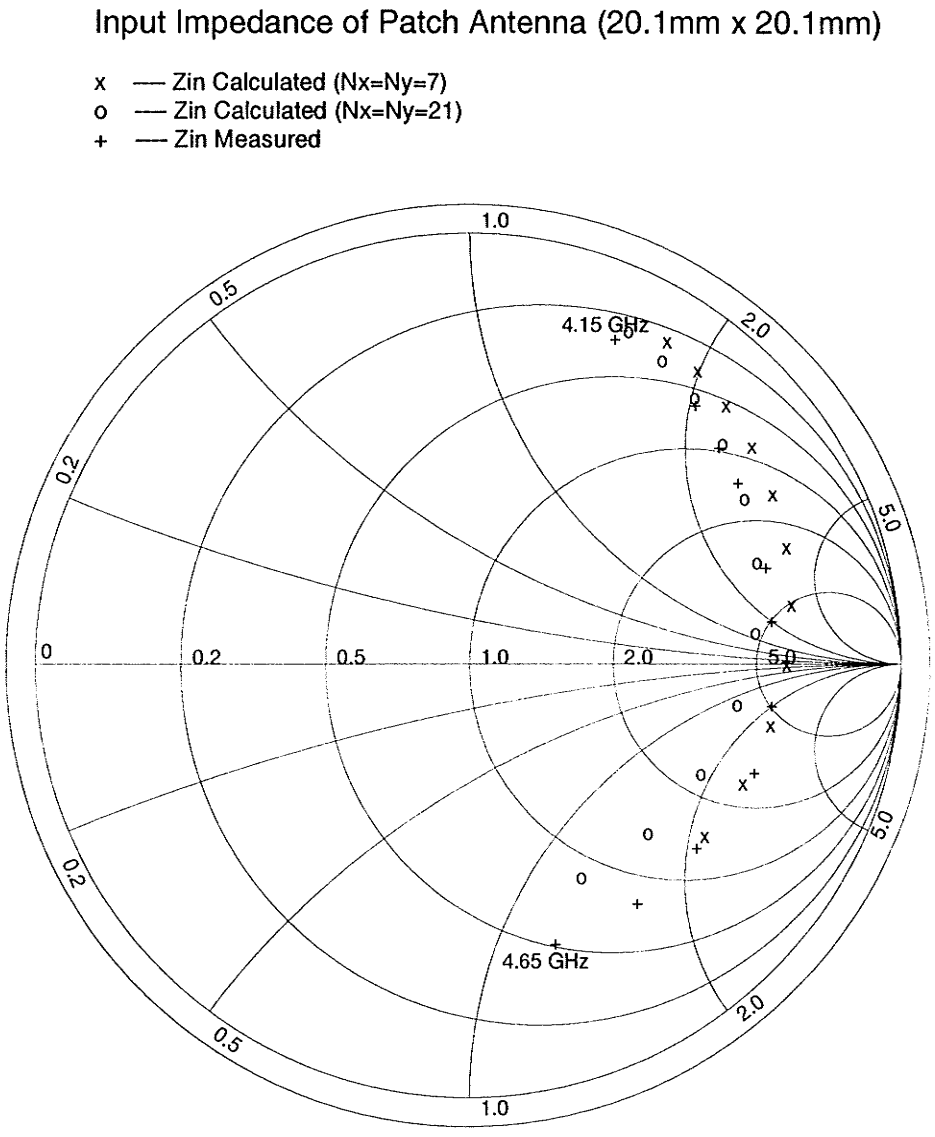

Fig. 5.5.2 Input Impedance for Patch Antenna Resonant at 4.30 GHz

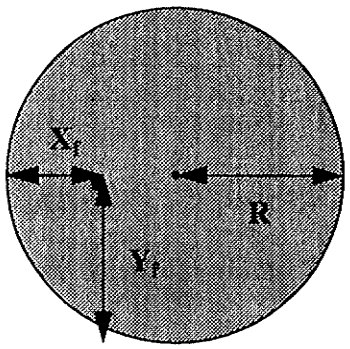

R = 18.8 mm
X_f = 4.7 mm
Y_f = 18.8 mm
ε_r = 2.60
tanδ = 0.0018
h = 1.60 mm

——— Nx =Ny =13
— — Nx =Ny = 21
— • — Measured

Real Part of Input Impedance vs. Frequency

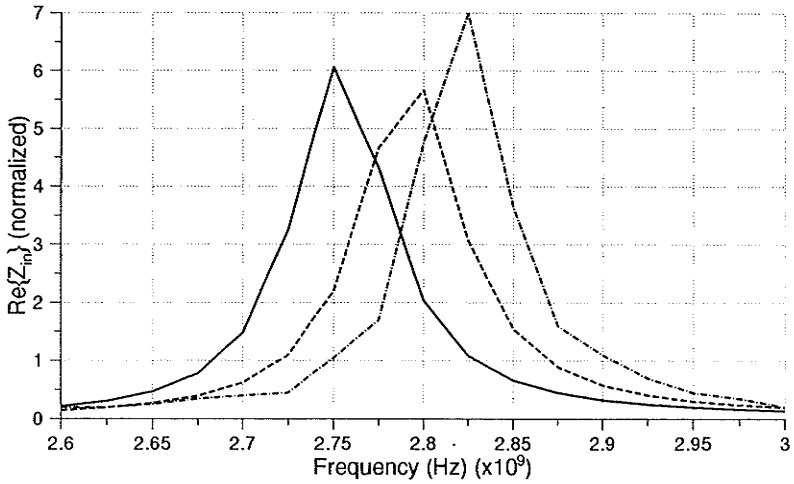

Imaginary Part of Input Impedance vs. Frequency

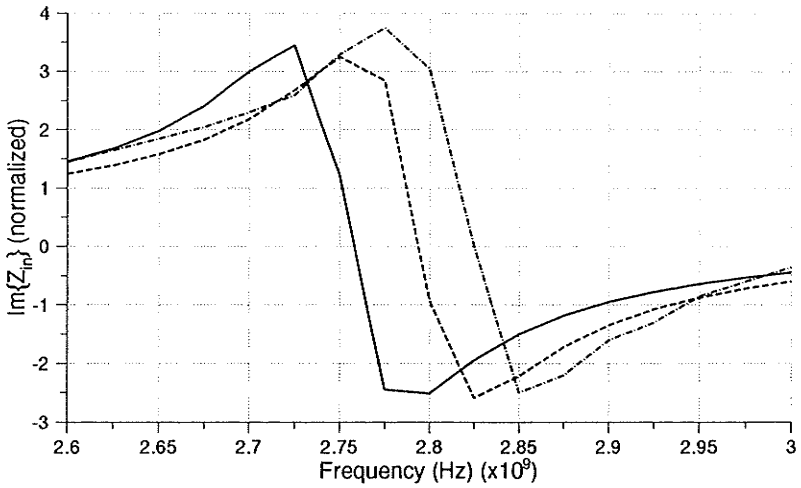

Fig. 5.5.3 Real and Imaginary Part of the Input Impedance of a Circular Disk Miscrostrip Antenna Operating at 2.80 GHz

5.6 Reactively Loaded Antennas

Placing a reactive load between the conducting surface and ground plane has been shown to create increased bandwidth when the load is placed properly with respect to the coaxial feed [40], or the addition of such a load can help to alter the input impedance seen by the feed, as the currents on the surface of the conductor will be adjusted, to provide a better match with the feed [10]. Circularly polarized radiation can also be obtained if the loading is used in conjunction with special feeding techniques [9].

The presented method is used to model the placement of reactive loads between the conducting surface and ground plane. Part of the objective of the method developed here is to be able to characterize different loading, as well a feeding configurations. In this sense, then, this type of device which has been studied also by Ali-Khan et al.[10] provides a good test as to the validity of this method for loaded microstrip structures. To confirm the generality, two different structures are studied. The first contains a single shorting pin the same distance from the nonradiating edge as the feed at a point presupposed to maintain the same resonant frequency but increase the bandwidth somewhat. The dimensions of the patch, along with the feed and load points are given in figures 5.6.1 and 5.6.2. The Smith Charts associated with each figure demonstrate the agreement with the result measured by Richmond. The Smith charts suggest that, in general, a coarse segmentation is not adequate for determining the quickly varying fields close to the load pin. Much better agreement is obtained, however, when the segmentation is increased by a factor of about 1.5. The second configuration consists of a the same patch loaded with two shorting posts, equally distant from the radiating edge. This decription and result is given in figure 5.6.3.

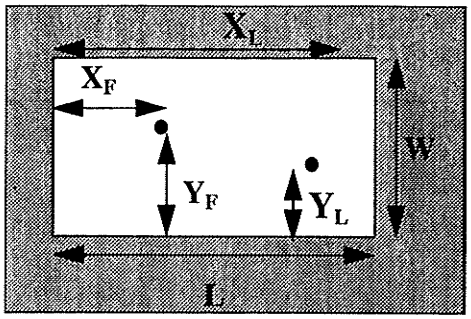

L = 60 mm
W = 40 mm
XF = 10 mm
YF = 10 mm
h = 1.58 mm
ε_r = 2.43

Reactively Loaded Patch (XL=25mm YL=9.1mm)

x —— Zin Measured
o —— Zin Calculated(Nx=9 Ny=6)
+ —— Zin Calculated (Nx=15 Ny=10)

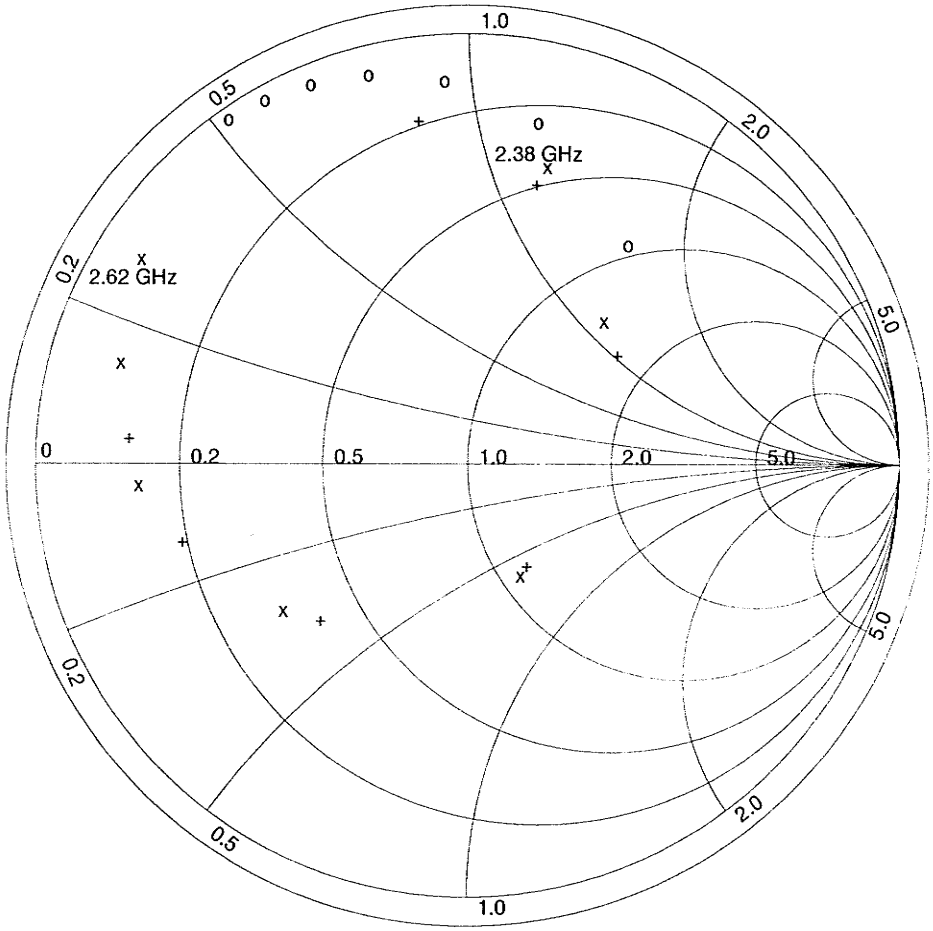

Fig. 5.6.1 Input Impedance of a Microstrip Patch Antenna Loaded with a Shorting Post at • (25.0mm.9.1mm)

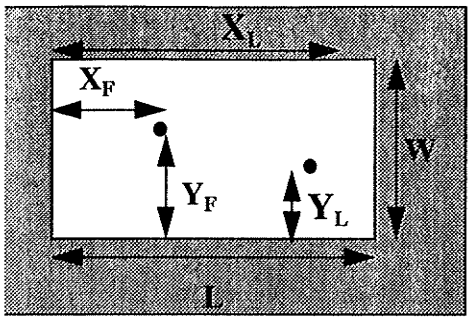

L = 60 mm
W = 40 mm
XF = 10 mm
YF = 10 mm
h = 1.58 mm
ε_r = 2.43

Reactively Loaded Patch (XL=17.5mm YL=10.5mm)

x — Zin Measured
o — Zin Calculated (Nx=9 Ny=6)
+ — Zin Calculated (Nx=15 Ny=10)

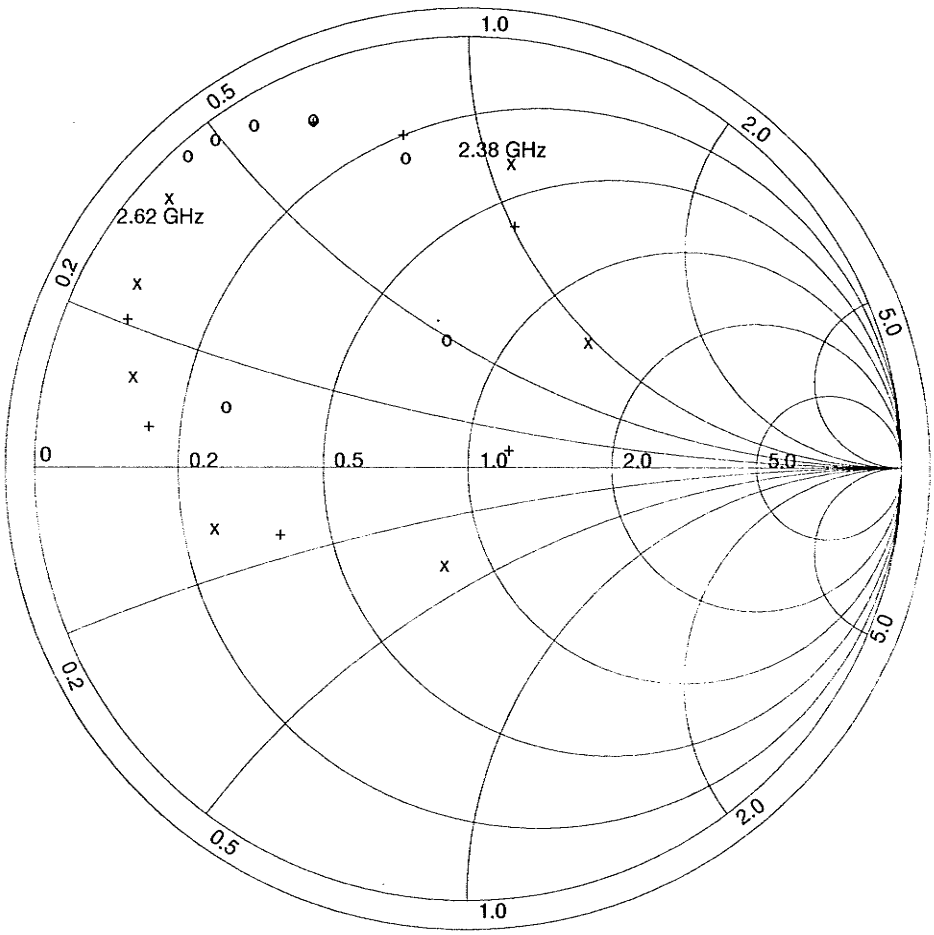

Fig. 5.6.2 Input Impedance of a Microstrip Patch Antenna Loaded with a Shorting Post at (17.5mm, 10.4mm)

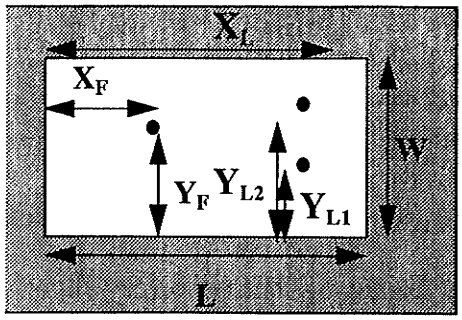

L = 60 mm
W = 40 mm
XF = 10 mm
YF = 10 mm
h = 1.58 mm
ε_r = 2.43
YL1 = 27.6mm
YL2 = 12.4mm
XL= 30 mm

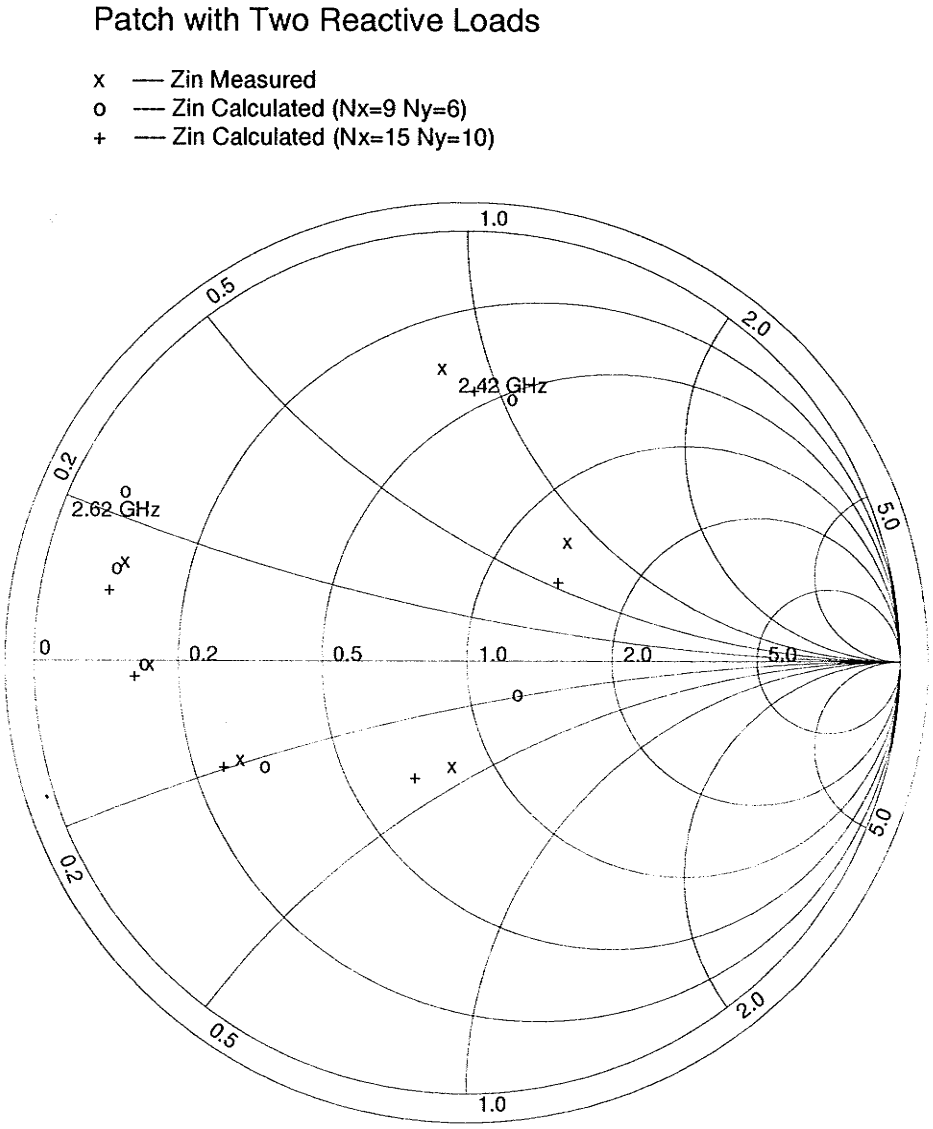

Fig. 5.6.3 Input Impedance of a Microstrip Patch Antenna Loaded with Two Shorting Posts

It is clearly demonstrated once again that the method is increasingly accurate with an increased segmentation. One reason for this, apart from the obvious reason that a finer segmentation is capable of more accurately modelling the current distribution on the patch, is that increased flexibility in the placement of the probe is realized. In the paper by Ali-Khan, the centre frequency is maintained by displacing the probe very slightly in the y-direction. An increased segmentation for the present method allows this displacement more accurately. Results with the increased segmentation scheme give results accurate within about 3% of the frequency.

6 Conclusions

6.1 Performance of the Method

It has been demonstrated that the input impedances calculated using the presented method have an agreement with measured results consistently within five percent for the examples shown in Chapter 5. Furthermore, the results for the radiated field are qualitatively in agreement when compared to measured and analytic results. Major problems of accuracy, however, do arise when the structure under analysis takes on an irregular shape. Structures with increasingly thick substrates may also cause some concern when the input impedance is to be studied. These problems may be alleviated by considering some of the suggestions made in the next section.

An additional problem is faced when trying to determine the effect of an increased discretization in the input impedance result. While it was demonstrated that an increased segmentation will provide a smoother current distribution in the case of a single line, the study of the effect on the input impedance is not trivial. Since the segmentation inherently determines which points the coaxial or microstrip feed may be situated at, an increased segmentation will alter the choices available for inserting the model feed. An attempt was made to create a more arbitrary expression for the fields near the feed probes and load points but this did not provide an adequate description of the conversion of probe currents to surface currents. The method suggested in the "Recommendations for Further Work" section in this chapter show more promise for solving this problem.

The tool that was developed using the formulation described in the first sections of this document will provide a relatively fast method of obtaining various parameters of interest to designers of microstrip antennas and circuits, approximately twenty minutes per frequency on a Sun Sparc2 workstation. The system memory required for the single precision version of the program is approximately 12 MBytes suggesting that this tool could also be easily ported to PC based system. Finally, the modular nature of the program code will allow the continuation of this work to include increasingly complex structures and increase the output capabilities when other parameters are to be considered.

6.2 Recommendations for Further Work

The structures that can be analysed using the Method of Moments as applied here are general but the accuracy becomes questionable for more irregular shapes. If the segmentation of the conducting surface is increased to the point of acceptible accuracy for such irregular structures, computer time and memory required may become unrealistically high. One way to improve this accuracy could to change the method of segmentation so that geometries could be modelled more accurately without significantly increasing the number of segments that are to be used. In addition to this fact, the current method is strict in its application of the feed and load points, more generality is required. A method for solving both issues may be to use triangular patches to discretize the conducting surface in place of the present rectangular ones. This method may also be useful for creating a mesh that is adaptive, using a coarse discretization where the variation in the fields and currents are small and increasing the segmentation where they vary more rapidly, close to the feeds, loads, and edges. The literature already shows some of this work being done [43].

Another level of complexity that is not included here is the addition of extra layers of dielectric substrate [37]. The most significant part of the adaptation to solve this type of problem would be to reformulate the Green's functions for the particular scheme of layers that is required. A combination of the triangular mesh and the Green's functions for multiple layers would act as an excellent tool for the analysis of a completely arbitrary microstrip structure.

One of the major, time exhaustive, operations of the analysis is the numerical calculation of the Green's functions. A closed form for the single layer format has recently been given by Chow et al. [44] and it may be possible to extend this formulation to multiple layers.

A last consideration is the fact that the current tool was written with a single precision floating point in order to save computation memory and time. If increasing accuracy without regard to computation time or memory is required, the effort required for a translation to double precision would be trivial.

References

[1] Hoffmann, R. K., "Handbook of Microwave Integrated Circuits", Artec House, Norwood, MA, 1987.

[2] Gupta, K. C., "Microwaves", Wiley Eastern Limited, New Delhi, 1979.

[3] Carver, K. R., Mink, J. W., "Microstrip Antenna Technology", *IEEE Trans. Antennas and Propagation* Vol. 29, pp 2-24, 1981.

[4] Lo, Y.T., Solomon, D. and Richards, W.F., "Theory and Experiment on Microstrip Antennas", *IEEE Trans. Antennas and Propagation*, Vol. 27, pp. 137-145, 1979.

[5] Pozar, D.M., "Input Impedance and Mutual Coupling of Rectangular Microstrip Antennas", *IEEE Trans. Antennas and Propagation,* Vol. 30, pp. 1191-1196, 1982.

[6] Chew, W.C. and Kong, J.A., "Radiation Characteristics of a Circular Microstip Antenna", *Journal of Applied Physics*, Vol. 51, No. 7, pp. 3907-3915, July 1980.

[7] Uzunoglu, N.K., Alexopolous, N.G., Fikioris, J.G., "Radiation Properties of Microstrip Dipoles", *IEEE Trans. Antennas and Propagation*, Vol. 27, pp. 853-858, 1979.

[8] Roerder, A.G., "The Cross Antenna: A New, Low Profile Circularly Polarized Radiator", *IEEE Trans. Antennas and Propagation*, Vol. 38, pp. 704-710, 1990

[9] Schaubert, D.H., Farrar, F.G, Sindoris, A. and Hayes, S.T., "Microstrip Antennas with Frequency Agility and Polarization Diversity", *IEEE Trans. Antennas and Propagation*, Vol. 29, pp. 118-123, 1981.

[10] Ali-Khan, A.,Richards, W.F., Long, S.A., "Impedance Control of Microstrip Antennas Using Reactive Loading", *IEEE Trans. Antennas and Propagation*, Vol. 37, pp. 247-251, 1989.

[11] Kumar, G and Gupta, K.C., "Nonradiating Edges and Four Edges Gap Coupled Multiple Resonator Broad-Band Microstrip Antennas", *IEEE Trans. Antennas and Propagation*, Vol. 33, pp. 173-178, 1985

[12] Kumar, G and Gupta, K.C., "Directly Coupled Multiple Resonator Wide-Band Microstrip Antenna", *IEEE Trans. Antennas and Propagation,* Vol. 33, pp. 173-178, 1985.

[13] James, J.R., Hall, P.S., Wood, C., "Microstrip Antenna Theory and Design", Peter Perigrinus, London, 1981.

[14] Birkeland, J. and Itoh,T., "Planar FET Circuits for Active Antenna Elements", *Proceedings of ISAP*, pp. 277-280, 1989.

[15] Navarro, J.A., Hummer, K.A., Cheng, K., "Active Integrated Antenna Elements", *Microwave Journal*, pp115-126, January 1991.

[16] Itoh, T., "Numerical Techniques for Microwave and Millimeter-Wave Passive Structures", Wiley, New York,1989.

[17] Hoefer, W.J.R., "The Transmission Line Matrix Method - Theory and Applications", *IEEE Trans. Microwave Theory and Techniques*, Vol. 33, pp. 882-893, 1979.

[18] Harrington, R.F. "Field Computation by Moment Methods", MacMillan, New York, 1967.

[19] Mosig, J.R. and Gardiol, F.E., "General Integral Equation Formulation for Microstrip Antennas and Scatterers", *IEE Proc.*, Vol. 132, Part H, pp.424-423, 1985.

[20] Harrington, R.F. "Time Harmonic Electromagnetic Fields", McGraw-Hill, New /York, 1961

[21] Jordan, E.C. and Balmain, K.G., "Electromagnetic Waves and Radiating Systems", Prentice-Hall, Englewood Cliffs, N.J., 1950.

[22] Mosig, J.R. and Gardiol, F.E., "A Dynamical Radiation Model for Microstrip Structures" in *Advances in Electronics and Electron Physics*; Hawkes, P. (Ed.) Vol. 59, Academic Press Inc., New York, NY, 1985

[23] Sommerfeld, A.N. "Partial Differential Equations in Physics", Academic Press Inc., New York, 1949.

[24] Mosig, J.R. and Gardiol, F.E., "Analytical and Numerical Techniques in the Green's Function Treatment of Microstrip Antennas and Scatterers", *IEE Proc.*, Vol. 130, Part H, pp. 175-182, 1983.

[25] Mosig, J.R.and Hall, R.C., "Vertical Monopoles Embedded in a Dielectric Substrate", Proc. IEE Vol. 136, Part H, December 1989

[26] Press, W.H., Teukolsky, S.A., Vellering, W.T., Flannery, B.P., "Numerical Recipes in C", Cambridge University Press, Cambridge, U.K., 1988.

[27] Mosig, J., "Integral Equation Technique", in *Numerical Techniques for Microwave and Millimeter-Wave Passive Structures,* Itoh, T. (Ed.), pp. 133-213, Wiley, New York, 1989.

[28] Sidi, A., "Numerical Evaluation of Very Oscillatory Infinite Integrals by Extrapolation", *Mathematics of Computation*, Vol. 38, pp. 517-529, April 1982

[29] Mahadevan, K. and Auda, H.A., "Electromagnetic Field of a Rectangular Patch of Uniform and Linear Distributions of Current", *IEEE Trans. Antennas and Propagation*, Vol. 37, pp. 1503-1509

[30] Popovic, B.D., Dragovic, M.B., Djordjevic, A.R., "Analysis and Synthesis of Wire Antennas", Research Press Studies, Chicester, U.K., 1982.

[31] Popovic, B.D., "Theory of Cylindrical Antennas With Lumped Impedance Loadings", *The Radio and Electronic Engineer*, Vol. 43, pp. 243-248, April, 1973.

[32] Burke, G.J. and Poggio, A.J., "Numerical Electromagnetics Code", Naval Ocean Systems Center, San Diego, 1977

[33] Sui,W., Christensen, D.A., Durney, C.H., "Extending the Two-Dimensional FDTD Method to Hybrid Electromagnetic Systems with Active and Passive Lumped Elements", *IEEE Trans. Microwave Theory and Techniques*, Vol. 40, pp. 724-730, 1992.

[34] Gillard, R.,Legay, H.,Floc'h, J.M.,Citerne, J., "Rigorous Modelling of Receiving Active Microstrip Antenna", *Electronics Letters*, Vol. 27, pp. 2357-2359, Dec. 1991.

[35] Mosig, J.R. and Gardiol, F.E., "Rayonnement d'une Antenne Microruban de Forme Arbitraire", *Annales de Telecommunication*, Vol. 40, pp. 181-189, 1985.

[36] Schaubert, D.H., Pozar, D.M., Adrian, A, "Effect of Microstrip Antenna Thickness and Permittivity: Comparison of Theories with Experiment", *IEEE Trans. Antennas and Propagation*, Vol. 37, pp. 677-682, June 1989.

[37] Legay, H. "Modelisation d'Antennes Imprimees Multicouches a Plusiers Gravures de Formes Quelconques", Ph.D. Thesis, INSA de Rennes, June 1991

[38] Pozar, D.M., "Input Impedance and Mutual Coupling of Rectangular Microstrip Antennas", *IEEE Trans. Antennas and Propagation*, Vol. 30, pp. 1191-1196, Nov. 1982

[39] Abboud, F, et. al., "Simple Model for the Input Impedance of Coax-Fed Rectangular Microstrip Patch Antenna for CAD", *IEE Proc.*, Vol. 135, Part H, pp. 323-326, 1988.

[40] Zhong, S.S. and Lo,Y.T., "Single Element Rectangular Microstrip Antenna for Dual Frequency Operation", *Electronic Letters*, Vol. 19, pp. 298-300, April 1983.

[41] Balanis, C.A., "Antenna Theory: Analysis and Design", Wiley, New York, 1982.

[42] Cheng, D.K., "Field and Wave Electromagnetics", Addison-Wesley, Reading, Mass, 1989.

[43] Kipp, R. and Chan, C.H., "Triangular Domain Basis Functions for Full-Wave Analysis of Microstrip Discontinuities", *IEEE Trans. Microwave Theory and Techniques*, Vol. 41, pp. 1187-1194, June/July 1993.

[44] Chow, Y.L., Yang, J.J., Fang, D.G., Howard, G.E.,"A Closed-Form Spatial Green's Function for the Thick Microstrip Substrate" *IEEE Trans. Microwave Theory and Techniques*, Vol. 39, pp. 588-592, March 1991.

Appendix A: Components of the Impedance Matrix

Basic Components of the Matrix

Test Element -x ; Source Element - x:

$$Z_{xx}^{ij} = \frac{1}{k_o}\left(\Gamma_V^H\left(\hat{r}_{xi}^{+} \middle| \hat{r}_{xj}^{+} \right) + \Gamma_V^H\left(\hat{r}_{xi}^{-} \middle| \hat{r}_{xj}^{-} \right) - \Gamma_V^H\left(\hat{r}_{xi}^{-} \middle| \hat{r}_{xj}^{+} \right) - \Gamma_V^H\left(\hat{r}_{xi}^{+} \middle| \hat{r}_{xj}^{-} \right) \right)$$

$$-k_o \int_{C_{xi}} \Gamma_A^{xx}(\hat{r}|\hat{r}_{xj})\, dx + j\frac{2\pi}{Z_o}(Z_s + Z_{Lxi})\frac{\Delta x}{\Delta y}\delta_{ij}$$

Where Z_{Lxi} is any load between charge cells connected by C_{xi} and δ_{ij} is unity when $i=j$ and is zero otherwise.. Note that the expresion for Z_{yy}^{ij} is identical with Δx and Δy exchanged and C_{yi} replacing C_{xi} ,

Test Element - x; Source Element - y:

$$Z_{xy}^{ij} = \frac{1}{k_o}\left(\Gamma_V^H\left(r_{xi}^{+} \middle| r_{yj}^{+} \right) + \Gamma_V^H\left(r_{xi}^{-} \middle| r_{yj}^{-} \right) - \Gamma_V^H\left(r_{xi}^{-} \middle| r_{yj}^{+} \right) - \Gamma_V^H\left(r_{xi}^{+} \middle| r_{yj}^{-} \right) \right)$$

Noting that $Z_{xy}^{ij} = Z_{yx}^{ji}$

Test Element - x ; Source Element - z:

$$Z_{xz}^{ij} = \frac{1}{k_o}\left(\Gamma_V^V\left(r_{xi}^{+} \middle| r_{zj}^{+} \right) + \Gamma_V^V\left(r_{xi}^{-} \middle| r_{zj}^{-} \right) - \Gamma_V^V\left(r_{xi}^{-} \middle| r_{zj}^{+} \right) - \Gamma_V^V\left(r_{xi}^{+} \middle| r_{zj}^{-} \right) \right)$$

Test Element - x ; Source Element - junction:

$$Z_{xj}^{ij} = \frac{1}{k_o}\left(\Gamma_V^H\left(\hat{\rho}_{xi}^{+}\middle|\hat{\rho}_{jj}^{+}\right) + \Gamma_V^V\left(\hat{\rho}_{xi}^{-}\middle|\hat{\rho}_{jj}^{-}\right) - \Gamma_V^H\left(\hat{\rho}_{xi}^{-}\middle|\hat{\rho}_{jj}^{+}\right) - \Gamma_V^V\left(\hat{\rho}_{xi}^{+}\middle|\hat{\rho}_{jj}^{-}\right)\right) - k_o \int_{C_{xi}} \Gamma_A^{xj}(\hat{\rho}|\hat{\rho}_{jj})\, dx$$

Similar expressions can be obtained for Z_{xj}^{ij} and Z_{xj}^{ij} by exchanging y for x in these two equations.

Test Element - z ; Source Element - x:

$$Z_{zx}^{ij} = \frac{1}{k_o}\left(\Gamma_V^H\left(\hat{\rho}_{xi}^{+}\middle|\hat{\rho}_{xj}^{+}\right) + \Gamma_V^H\left(\hat{\rho}_{xi}^{-}\middle|\hat{\rho}_{xj}^{-}\right) - \Gamma_V^H\left(\hat{\rho}_{xi}^{-}\middle|\hat{\rho}_{xj}^{+}\right) - \Gamma_V^H\left(\hat{\rho}_{xi}^{+}\middle|\hat{\rho}_{xj}^{-}\right)\right) - k_o \int_{C_{zi}} \Gamma_A^{zx}(\hat{\rho}|\hat{\rho}_{xj})\, dx$$

Test Element - z ; Source Element - z:

$$Z_{zz}^{ij} = \frac{1}{k_o}\left(\Gamma_V^V\left(\hat{\rho}_{zi}^{+}\middle|\hat{\rho}_{zj}^{+}\right) + \Gamma_V^V\left(\hat{\rho}_{zi}^{-}\middle|\hat{\rho}_{zj}^{-}\right) - \Gamma_V^V\left(\hat{\rho}_{zi}^{-}\middle|\hat{\rho}_{zj}^{+}\right) - \Gamma_V^V\left(\hat{\rho}_{zi}^{+}\middle|\hat{\rho}_{zj}^{-}\right)\right)$$

$$-k_o \int_{C_{zi}} \Gamma_A^{zz}(\hat{\rho}|\hat{\rho}_{zj})\, dx + j\frac{2\pi}{Z_o} Z_{Lzi} \frac{\Delta x}{\Delta y} \delta_{ij}$$

Test Element - z ; Source Element - junction:

$$Z_{zj}^{ij} = \frac{1}{k_o}\left(\Gamma_V^H\left(\hat{\rho}_{zi}^{+}\middle|\hat{\rho}_{zj}^{+}\right) + \Gamma_V^V\left(\hat{\rho}_{zi}^{-}\middle|\hat{\rho}_{zj}^{-}\right) - \Gamma_V^H\left(\hat{\rho}_{zi}^{-}\middle|\hat{\rho}_{zj}^{+}\right) - \Gamma_V^V\left(\hat{\rho}_{zi}^{+}\middle|\hat{\rho}_{zj}^{-}\right)\right)$$

$$-k_o \int_{C_{zi}} \Gamma_A^{zz}(\hat{\rho}|\hat{\rho}_{zj})\, dx - \int_{C_{zi}} \Gamma_A^{zj}(\hat{\rho}|\hat{\rho}_{jj})\, dx$$

When the test element corresponds to a junction, the expressions for the z directed test segments hold as a junction test segment is simply a z directed segment located near the surface of the dielectric.

Matrix Components Corresponding to Active Elements

Test Element -x ; Source Element - device port:

$$Z_{xd}^{ij} = \frac{1}{k_o}\left(\Gamma_V^H\left(\hat{r}_{xi}^{+}\middle|\hat{r}_{dj}\right)-\Gamma_V^H\left(\hat{r}_{xi}^{-}\middle|\hat{r}_{dj}\right)\right)-k_o\int_{C_{xi}}\Gamma_A^{xj}(\hat{r}|\hat{r}_{dj})\,dx$$

Test Element - device port; Source Element - x:

$$Z_{dx}^{ij} = \frac{1}{k_o}\left(\Gamma_V^H\left(\hat{r}_{di}\middle|\hat{r}_{xj}^{+}\right)-\Gamma_V^H\left(\hat{r}_{di}\middle|\hat{r}_{xj}^{-}\right)\right)-k_o\int_{-h}^{0}\Gamma_A^{zx}(\hat{r}|\hat{r}_{xj})\,dz$$

Test Element - device port; Source Element - device port:

$$Z_{dd}^{ij} = \frac{1}{k_o}\Gamma_V^H(\hat{r}_i|\hat{r}_j)-k_o\int_{-h}^{0}\Gamma_A^{zj}(\hat{r}|\hat{r}_{dj})\,dz+j\frac{2\pi}{Z_o}Z_{ij}$$

Where Z_{ij} is the ij component of the unnormalized Z matrix of the device.